Physical simulation of microstructure and texture evolution in extrusion of selected 6xxx aluminum alloys

Van Geertruyden, William H.

Physical Simulation of Microstructure and Texture Evolution in Extrusion of…

June 2000

Physical Simulation of Microstructure and Texture Evolution in Extrusion of Selected 6xxx Aluminum Alloys

by

William H. Van Geertruyden

A Thesis

Presented to the Graduate and Research Committee

of Lehigh University

in Candidacy for the Degree of

Master of Science

in

Materials Science and Engineering

May 4, 2000

CERTIFICATE OF APPROVAL

This thesis is accepted and approved in partial fulfillment of the requirements for the Master of Science

May 4, 2000

Date

Wojciech Z. Misiolek
Thesis Advisor

David B. Williams
Chairperson

ACKNOWLEDGEMENTS

I would like to express my gratitude to the following individuals and organizations for their guidance and assistance during the formulation of this thesis. This research would not have been possible without the financial support in the form of a grant from The Aluminum Association. I would like to thank all the members of the Academic Committee from The Aluminum Association Extrusion Products Division who oversaw this research, especially John Faunce, Rob Akans, Walt Cebulak, and John Green. Also, billet material from Werner Co., Ormet Corp. and Easco Aluminum was vital to this research. The knowledge and help from both Greg Lea and Richard Kelly from Werner Co. were also invaluable.

I would also like to thank the following individuals: Arlan Benscoter for his help and instruction in metallography during this research and Jesse Nawrocki for his training and ingenuity on Gleeble simulation. Also thanks to fellow graduate students Alex Bandar, Steve Claves, and Kai Lorcharoensery for their support and help and Jennifer Braggin whose help was undying and generous as a work study student. I would also like to thank my advisor Dr. Wojciech Z. Misiolek for his excellent guidance during this research. Finally, I would like to thank my parents and my two wiser brothers, Yann and Peter, for their love and support.

TABLE OF CONTENTS

List of Tables

List of Figures

ABSTRACT

In modeling of the extrusion process for aluminum alloys, several techniques can be used. In this research, physical simulation is performed using a thermal mechanical simulator. This simulator is capable of replicating the thermal cycles that a material undergoes during a deformation process. By utilizing resistive heating and water-cooled grips, thermal cycles can be accurately reproduced in terms of heating and cooling rates. Thermal cycles of 6xxx series alloys were studied in terms of varying preheat and extrusion temperatures and determining the effect on microstructure and mechanical properties. It was found that higher temperatures in the preheat and extrusion cycles are ideal to produce a solutionized structure after extrusion and displayed the best mechanical properties. The low preheat – low extrusion thermal cycles retained coarse precipitates after extrusion and ageing and displayed the worst mechanical properties.

In addition, compression testing is used to model the deformation and texture evolution at certain temperatures, strains, and strain rates. The advantage of compression testing is the presence of friction and that relatively high strains can be produced. Crystallographic characterization involved using a technique known as Electron Backscatter Diffraction (EBSD), which can determine texture information on a grain by grain basis. It was determined that there exists a change in deformed grain orientation from <110> to <111> at higher strains.

1.0 INTRODUCTION

1.1 Aluminum Extrusion Background

1.1.1 Extrusion Process Fundamentals

The process of metal extrusion involves forcing a block of material, usually cylindrical, through a fixed die in order to reduce its cross sectional area. The resultant shape of the extrudate will depend on the shape of the die orifice through which the material is forced. In extrusion, this reduction in cross sectional area is known as the extrusion ratio, which is the ratio of cross sectional area of the upset extrusion billet to that of the extruded product. A schematic representation of the process, both direct and indirect, is shown in Figure 1. Direct extrusion is the case whereby the ram travels in the same direction as the metal flow out of the die orifice. In indirect extrusion, the ram is pushing the die in the opposite direction of the metal flow. Important components of an extrusion press include the ram, die, container, dummy block, and die holder. Common metals and alloys that are extruded include copper, aluminum, brass, titanium, zirconium, and steel. In extrusion of aluminum alloys specifically, common alloys include 2xxx, 5xxx, 6xxx, and 7xxx series. The focus of this research is on 6xxx series aluminum alloys, which encompass the bulk of the aluminum extrusion industry. The demands of the market to produce more complex shapes and improved mechanical properties has made the importance of controlling process conditions of 6xxx alloys more important than ever.

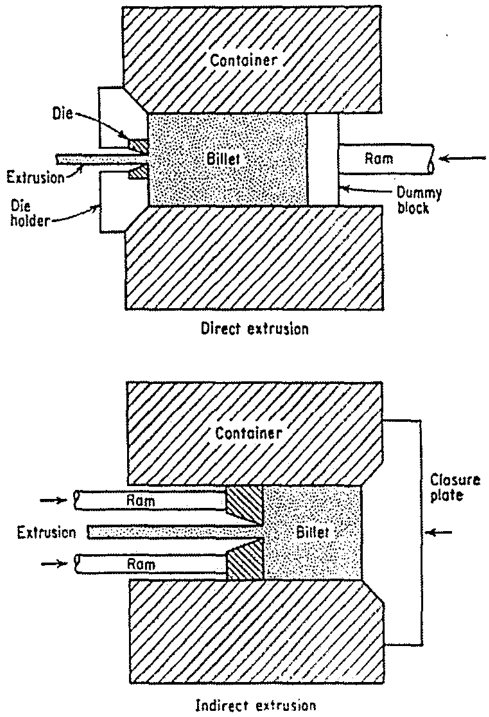

Figure 1: Schematic representation of direct and indirect extrusion processes.[1]

1.1.2 Process Simulation

In order to optimize the aluminum extrusion process, several conditions must be resolved. Industrial trials could be performed on an industrial press on a certain alloy and profile, which will accurately provide important information such as maximum exit speed and temperature. However, this method is often time and cost intensive because production on a press must be suspended. Numerical simulation, such as Finite Element Modeling (FEM), can be used whereby certain processing conditions, such as strain and temperature can be predicted for certain die geometries. However, this method is mostly limited to the two – dimensional case and usually does not take into account microstructural or textural evolution during extrusion. A laboratory model, which predicts microstructure, texture, and mechanical properties must be developed and subsequently scaled – up to industrial levels in order to be worthwhile. In this research, physical simulation is used in order to predict the effect of changing certain operating conditions and their influence on material response in order to optimize the process. These conditions include: temperature, heating and cooling rate, strain and strain rate. Physical simulation in this research is performed using a Gleeble thermal – mechanical simulator, which accurately replicates times, temperatures and stresses that a material undergoes during extrusion. It is important that all facets of the extrusion process be taken into account including their interactions. If results are obtained piecemeal, the effect of the other parts of the process will not be revealed. In this way, the Gleeble is capable of simulating an entire thermal cycle from homogenization to ageing more accurately than any laboratory furnace and more cost effectively than an industrial line, which has a number of different furnaces and a press.

1.1.3 6xxx Aluminum Alloy Metallurgy

The two types of alloys that will be investigated in this research are 6063, 6061. These are heat treatable alloys that can be used in the wrought or cast condition. The 6xxx alloys make up a majority of the aluminum extrusion industry because of their good combination of properties and relative ease to extrude. For example, 6xxx series alloys display good corrosion resistance, good formability, and good mechanical properties when compared to other aluminum alloys. The major alloying constituents of the 6xxx series alloys are magnesium and silicon. These elements combine to form the metastable hardening phase Mg_2Si. The precipitation sequence of Mg_2Si has been studied in depth, especially in terms of peak effectiveness on age hardening.[2] Starting from the supersaturated solid solution, upon ageing, the magnesium and silicon cluster together to form GP zones. Next, β'' Mg_2Si is formed as coherent Widmanstatten needles which lie in the [100] crystallographic directions. The β'' next forms into semi - coherent β' rods. The β' is associated with the maximum ageing strength obtainable because it is semi – coherent. B' semi – coherent laths are subsequently formed and are favored by high Si:Mg ratios. Finally, β Mg_2Si platelets are formed which may transform directly from β'. An example of a β Mg_2Si precipitate can be seen in Figure 2. In addition to being a precipitation hardening alloying element, both Mg and Si act as solid solution strengtheners. As will be discussed in depth later, the thermal cycles that an aluminum billet undergoes during the entire extrusion process strongly affects which form of the Mg_2Si phase is present. The morphology, distribution, and size of these precipitates strongly affect mechanical properties of the alloy and, hence, affect productivity. This becomes an issue when the flow stress of the material during extrusion may be too high because these elements are in solution. On the other hand, if the wrong form of Mg_2Si (coarse and inhomogeneously distributed) is present in the final aged microstructure, mechanical properties of the product will be compromised.

Other constituents that make up these alloys include copper in trace amounts for solid solution strengthening, and chromium and zirconium to raise the recrystallization temperature.[3] Zirconium and titanium are also added as grain refiners.[3] Iron is a naturally occurring impurity in aluminum alloys and forms the brittle α AlFeSi phase in 6xxx alloys during casting. Manganese is added to aid in the transformation of the α AlFeSi to the rounded β phase upon homogenization.[3] Hydrogen content, which has been linked to blister formation, is kept to a minimum. A summary of constituent make – up for some 6xxx series alloys is shown in Table I.

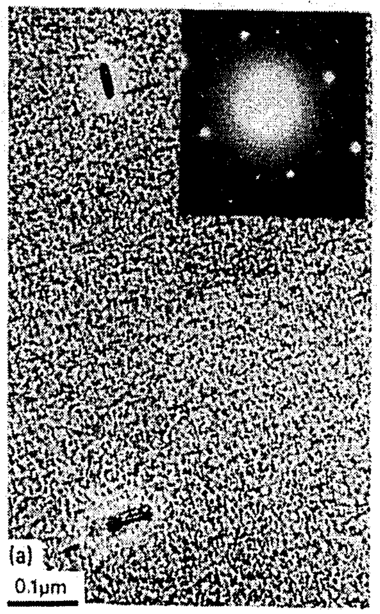

Figure 2: TEM image of needle shaped β - Mg_2Si in a 6xxx series alloy growing along [100] directions.[3]

There are many differences between 6063 and 6061 alloys, the main difference being the composition. 6061 is a more highly alloyed material and contains significantly higher Mg and Si contents. Consequently, the sensitivity of Mg_2Si forming under certain conditions is more of an issue than it is for a 6063 alloy. There are also differences in mechanical properties between 6xxx alloys as can be seen in Table II.

Table I: Alloying composition limits of selected 6xxx series alloys.[4]

Alloy Designation	Si	Fe	Cu	Mn	Mg	Zn	Cr	Ti
6061	0.4–0.8	0.7	0.15 – 0.40	0.15	0.8-1.2	0.25	0.04-0.35	0.15
6063	0.2-0.6	0.35	0.1	0.1	0.45-0.9	0.1	0.1	0.1
6105	0.6-1.0	0.35	0.1	0.03	0.35-0.8	0.1	0.03	..

Depending on the desired properties, heat treatable aluminum alloys can undergo several types of thermal ageing treatments known as tempers. The designation for tempers is as follows: F - as fabricated, O - annealed, W - solution heat treated, and T - thermally treated. In ageing, several tempers are pertinent. In this research, the T6 temper was used, which involves solution heat treating followed by a artificial ageing. For most 6xxx series alloys, a separate solution treatment is not necessary due to a press quench after extrusion. Depending on the alloy, a press quench can include "solid water" (extrudate passes through container of water), air, or water mist. Press quenching is used to keep the magnesium and silicon in solution so that no precipitation occurs before the ageing step. This is to ensure that the desired uniform distribution of fine precipitates occurs each time. For most 6xxx alloys, the usual T6 temper is performed at 178 ^{0}C (350^{0}F) for at least 6 hours.[3]

Table II: Mechanical properties of selected 6xxx alloys and tempers.[4]

Alloy and Temper	UTS (ksi)	YS (ksi)	Elongation (%)	Brinell Hardness
6063 – 0	13	7	..	25
6063 – T6	35	31	12	73
6061 – 0	18	8	25	30
6061 – T6	45	40	12	95

1.1.4 Thermal Simulation

The time and temperature that an aluminum billet sees during extrusion strongly affects its resultant extrudate properties and appearance, as well as its behavior during forming. Therefore, optimization of the thermal cycles that the material undergoes is crucial to improve productivity. A schematic diagram depicting the thermal cycles encountered throughout the entire extrusion process is shown in Figure 3.

The material is first cast from the liquid melt using casting techniques such as air – slip, hot – top, and direct chill (DC) casting. The importance of a high quality as – cast ingot is often overlooked and has been shown to greatly affect extrusion performance.[6] Several features occur in casting and must be optimized. Inherent in the casting process are dendrites which occur due to constitutional supercooling.

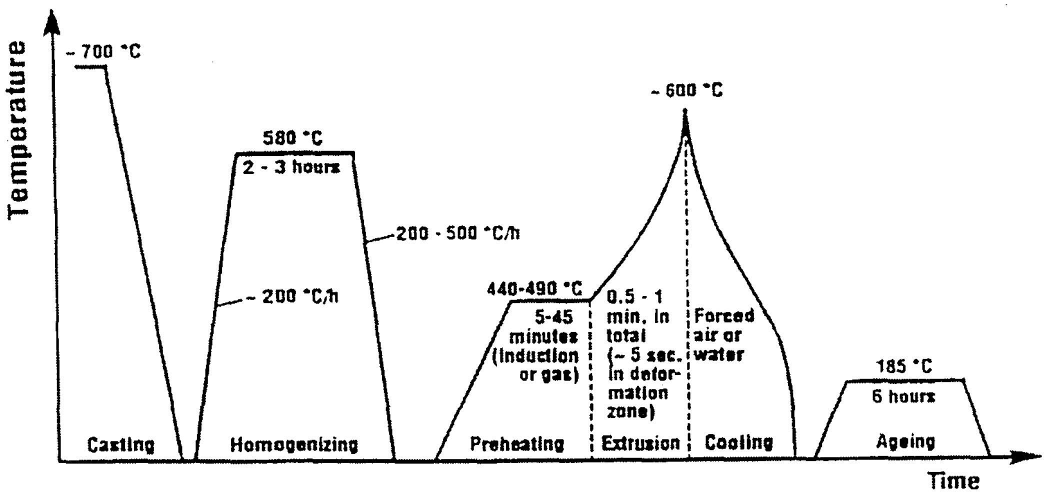

Figure 3: Temperature – Time profile of a 6xxx aluminum extrusion thermal history showing all stages of production from casting to ageing. [5]

In DC casting, a shell zone forms, which is the area in the periphery of the ingot that is solute rich at the surface and solute depleted further in. The goal of casting is to produce an ingot with uniform dendrite arm spacing (DAS), surface segregation, and shell zone thickness.[6] Also, the surface quality of the ingot is very important, and has been linked to poor surface quality of the extrudate.[6] After the ingot is cast, it is subsequently homogenized in a large furnace. The main goal of homogenization is to desegregate the microstructure. In 6xxx aluminum alloys, homogenization provides other uses. First, magnesium and silicon are forced into solution at the homogenization temperature. When the ingots undergo a specific cooling rate, a desired amount of magnesium and silicon precipitate as Mg_2Si, magnesium silicide. The cooling rate after homogenization is very important because the correct amount of Mg_2Si that precipitates is determined during this period. The amount of Mg_2Si that is present during preheating affects the flow stress of the material during extrusion. Next, during homogenization, the iron phase in 6xxx alloys, AlFeSi, is transformed from the brittle, needle shaped β phase to the more desired and rounded α phase.[7]

After homogenization, the ingots are cut into billets approximately 3 feet in length depending on the size of the extrusion press. Before extrusion takes place, the billets are preheated for two main reasons. First, extrusion in this case is a hot deformation process. In order to reduce the flow stress, the billets are sent through either a gas or induction furnace for approximately 5 to 30 minutes, depending on the furnace type and alloy. The second reason for preheating is to bring a majority of magnesium and silicon into solution before extrusion takes place. If too much magnesium and silicon are in solution, the flow stress is increased due to solid solution strengthening, and extrusion performance is compromised.

After preheating, the billet is automatically transferred to the extrusion container. If there is a lag in the transfer between the preheat furnace and the container, the microstructure may be affected.[8] The billet is then automatically transferred to the extrusion container and it is pressed through the die. The temperature change that takes place along the length of the billet as it is extruded is not uniform. Because of friction between the billet and the container and die, the temperature of the billet increases. The temperature also increases because of deformation heating. The literature reports that the temperature of the billet will increase by 100 ^{0}C in approximately 0.5 – 1.0 minutes.[5] Isothermal extrusion is a technique that has been recently developed which involves preheating the billet just before extrusion so that it contains a thermal gradient.

This thermal gradient is such that the front of the billet, which enters the extrusion chamber first, is warmer than the back. Therefore, during extrusion, the temperature rise due to deformation and friction will be even throughout the billet. Other advances in extrusion quality control include extrusion presses controlled by computer programs such as CADEX (Computer Aided Direct Extrusion), which accurately predicts and controls the maximum ram speed and billet temperature during extrusion.[9]

Once the material exits the die, it can be cooled several ways, depending on the alloy and desired properties. The exiting material can either be water quenched, air cooled by fans, or sent through a water mist. The temperature of the extrudate is closely monitored as it exits the die. Finally, after the extrudate is stretched to straighten it and to relieve any residual stresses, if the material is age – hardenable, it is sent to an ageing furnace. Again, the temperature and time that an extrudate is aged depends on the alloy and the type of properties that are desired. Ageing temperatures are usually in the range of 150 – 200 ^{0}C (300 to 400^{0}F) for more than six hours.[3] The heating rate and cooling rate of this process is not as vital to the constituent make - up.

1.1.5 Extrusion Limit Diagrams

The maximum temperature and speed at which a billet can be extruded without defects can be displayed in extrusion limit diagrams. An example of a limit diagram for a 6xxx alloy is shown in Figure 4. The diagram plots extrusion speed vs. billet temperature. The left-hand side of the plot is limited by the maximum allowable pressure that the alloy can be extruded at. Important factors that affect the pressure are extrusion ratio, the shape complexity, and the amount of Mg and Si in solution. The right hand side of the limit diagram is limited by the maximum allowable temperature that the alloy can be extruded at. Important factors affecting the maximum temperature deal with the surface quality, onset of surface defects, and alloy composition itself. The maximum temperature is incipient melting in the alloy. Where the two curves intersect is where the theoretically maximum temperature of extrusion exists. The objective is to create isothermal deformation at this optimum temperature.

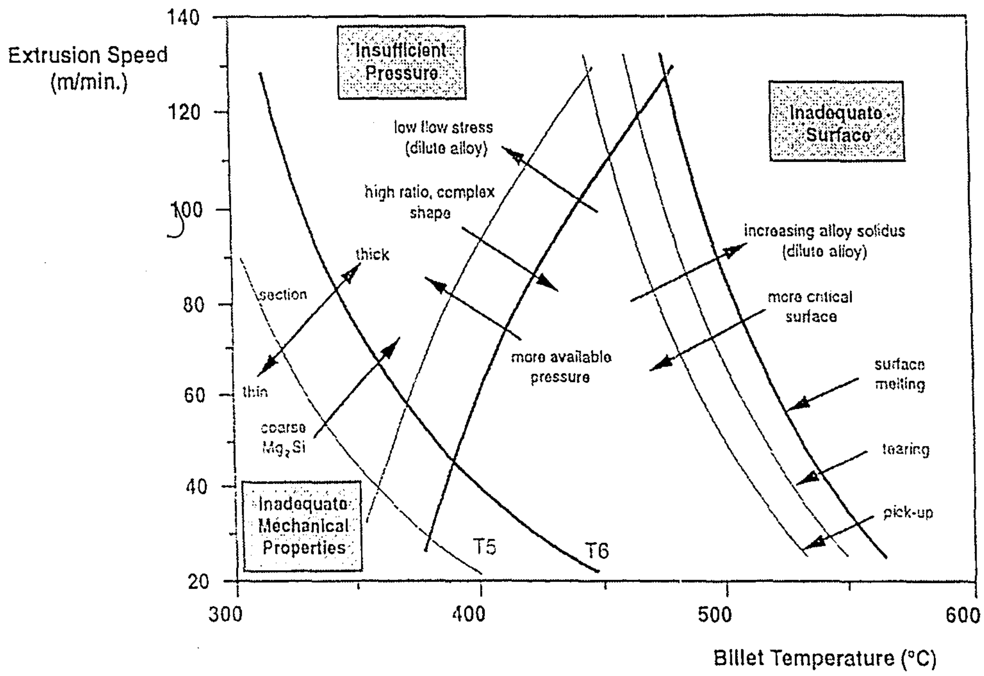

Figure 4: Extrusion limit diagram for a 6xxx aluminum alloy.[10]

1.1.6 Metal Flow

As the ram pushes the material through the die, the resultant metal flow is not uniform. In other deformation processes such as drawing and rolling, the deformation is much more homogeneous and symmetrical. Inherent in the process of extrusion is a series of deformation zones. These deformation zones exhibit variability in strain, strain rate, and temperature. Zones of deformation in extrusion include the dead metal zone, shear intensive zone, and main deformation zone close to the die orifice. This can be seen in Figure 5.

The dead metal zone results from the metal flowing into the corners at the die end of the container and becoming stagnant. The main deformation zone close to the die experiences a hydrostatic state of stress. The shear zone consists of the high strain region between the dead metal zone and main deformation zone. Macroscopic shear occurs in this region and high temperature increases result. Dynamic recrystallization may occur in this region due to this high temperature increase as can be seen in Figure 5.

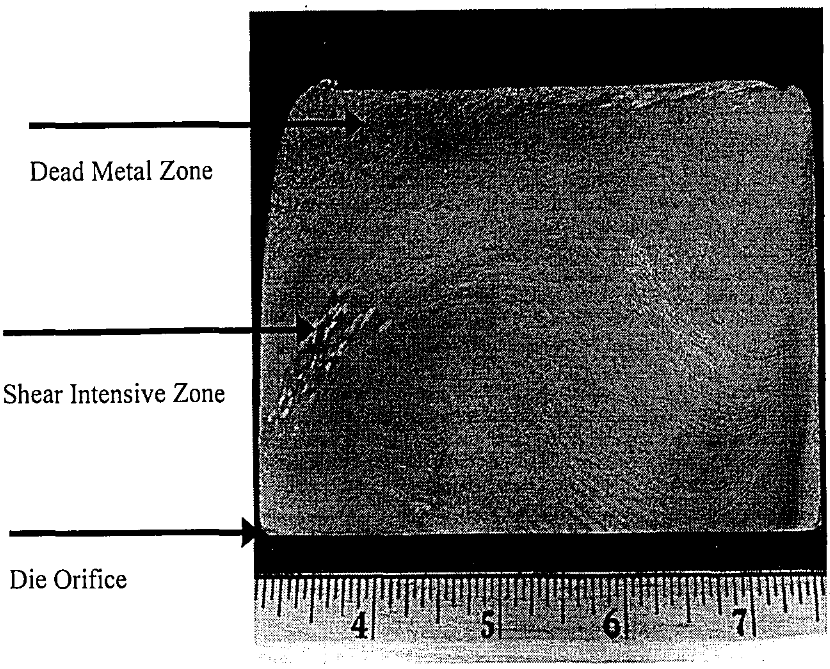

Figure 5: Example of metal flow in half of a 6105 alloy billet after it was partially extruded. Notice the shear and dead zone close to the die orifice.[11]

Several techniques have been used in the past to model and predict the flow pattern of material in extrusion. Gridded wax and plasticine billets have been extensively used to predict the flow using different die designs. The advantages of this method are that it is quick and relatively inexpensive.[12] Also, different die geometries and shapes can be easily machined into polymer dies. Several types of metal flow have been categorized using this method and are shown in Figure 6-i.[13] Type S flow is characterized as the most uniform flow with most of the deformation occurring directly in front of the die. This type of flow only occurs when there is no friction at the container wall, such as in glass lubricated metal extrusion. Type A flow is characterized as one in which the dead metal zone is more defined as a result of more friction at the die surface. Examples of Type A flow occur in lubricated extrusion of Pb, Sn, Bi, and Al. Type B flow is characterized as having increased friction at the container wall and a decreasingly homogeneous flow pattern. Examples of Type B flow occur in unlubricated Pb, Sn, Bi, Al and Al alloys. Finally, type C flow is characterized by a very large dead zone extending towards the back of the container. Type C flow is known to occur in extrusion of Brass, Mg, Al and Al alloys, and Sn with a radial temperature gradient. Valberg has recently introduced new flow patterns, which are shown in Figure 6-ii.[14] A more recent method used to predict metal flow is Finite Element Modeling (FEM). The advantage of this method is that it can accurately predict strain, strain rate and temperature information for given die shapes and geometries relatively fast. Unfortunately, the technology is still limited to two dimensions in most cases and relatively simple product geometry.

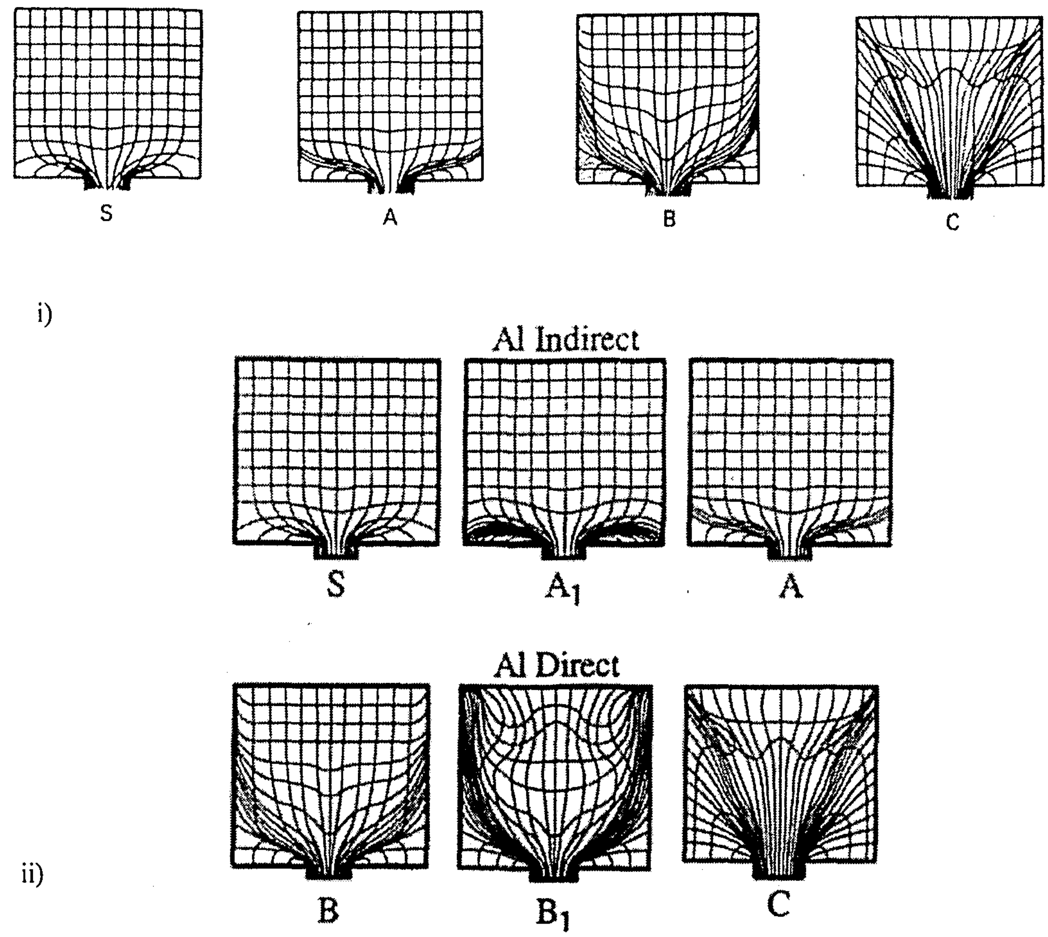

Figure 6: i) Examples of different types of metal flow seen in extrusion.[13]
ii) Adjusted flow patterns, A_1 and B_1 by Valberg.[14]

1.1.7 Selected Defects in Extrusion

Several defects occur during the extrusion process that limits its productivity and usefulness. The most common defect seen in extrusion is termed the extrusion defect or funnel effect. This defect occurs when the center of the billet travels faster than the edges of the billet through the die because of friction at the container wall. The result is a hollow which forms at the back of the billet and extends into the extrudate.[15]

Surface defects during extrusion include orange peel, pick – up, drag marks, cold shut, and tearing.[6] Reiso et al concluded that surface tearing was the result of tensile fracture due to incipient melting of certain eutectics.[16] These phases included Mg_2Si, and AlFeSi. Surface tearing occurs in two cases. Type I tearing occurs when the temperature of the surface of the extrudate exceeds the incipient melting point of certain phases at the surface. Type II tearing occurs in the matrix of the extrudate. These two cases can be seen in Figure 7. The objective is to create a situation where the maximum extrusion speed can be increased while at the same time reducing the degree of defects.

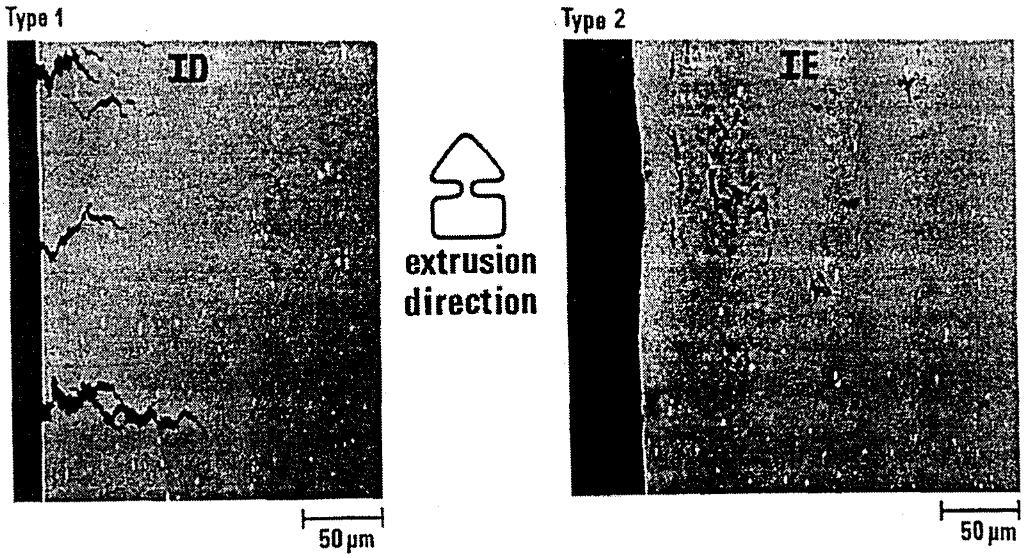

Figure 7: Tearing initiation caused at the extrudate surface (Type I) and sub – surface (Type II).[16]

1.2 Modeling of Microstructure Response to Processing Parameters

1.2.1 Gleeble Equipment and Theory

The equipment used for physical simulation in this research is a Gleeble 1000 HAZ thermal mechanical simulator manufactured by Dynamic Systems, Inc. The Gleeble uses resistive heating to accurately control the temperature of a sample using a closed - loop temperature feedback control that monitors the temperature of the sample several times per second. Depending on the programmed temperature, the sample can be rapidly heated, kept at a constant temperature, and be subsequently cooled at a controlled rate. In this way, the Gleeble can replicate all stages of an extrusion thermal cycle from homogenization to preheating, deformation heating, press quenching, and finally ageing. Traditional laboratory furnaces are not capable of replicating these temperatures and rates as accurately and representative of the extrusion process.

In addition to temperature control, the Gleeble also uses a servo – hydraulic ram to impart tensile or compressive loads on the sample during thermal cycling. In simulation of deformation in extrusion, several conditions must be met. These criteria include predicting maximum extrusion speed, mechanical properties, surface quality and structure. Compression testing has been used to model deformation in extrusion because of their similarities, such as presence of friction, different deformation zones, and therefore strain gradients.[17] This method also has the advantage that it allows for higher strains than tensile testing. Compression testing results in a similar state of stress compared with extrusion. In this manner, crystallographic analysis can be performed on a compression sample to study its deformation and relate the results to extrusion on an industrial press. In this way, for a given set of processing conditions, such as temperature, strain rate, and strain, the crystallographic information of different zones of deformation can be measured and analyzed. These different zones in a deformed billet include the dead metal zone, shear zone and main deformation zone close to the die. Friction between the billet and the die and container causes inhomogeneous deformation and redundant work. In Gleeble compression testing, the material close to the jaws is constrained which causes barreling as seen in Figure 8. The region in the middle of the sample is free to move laterally in the direction perpendicular to the compression axis. Consequently, secondary tensile stresses develop at the surface of the barreled region.

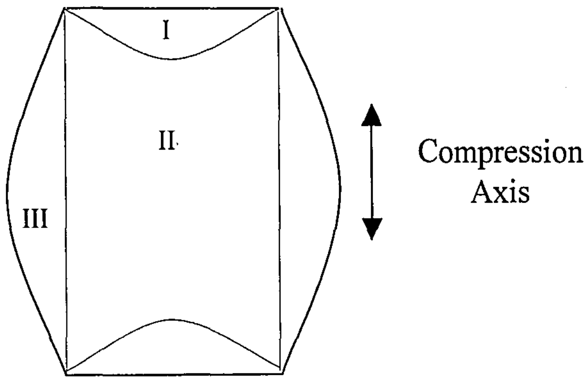

Figure 8: Schematic representation of compression sample showing different zones of deformation. Increasing strain is seen from zones I to III.

Zone I is a relatively strain free part of the sample due to the constraint between the sample and the jaws which resembles the dead metal zone in extrusion. Zone II is an area of increasing strain resembling the deformation zone near the die orifice. Zone III is a region of large strains corresponding to similar deformation in the shear intensive zone.

1.3 Characterization Methods

1.3.1 Electron Backscatter Diffraction

In order to fully characterize the material that is deformed, classical metallography can only go so far as to determine the microstructure. This includes grain size and morphology, precipitate distribution, etc. However, a relatively new technique, Electron Backscatter Diffraction (EBSD), has been developed which is a powerful tool that combines microstructural and crystallographic information. EBSD involves using a traditional Scanning Electron Microscope (SEM) to generate electrons that strike a tilted specimen and produce forward scattering electrons. Depending on the crystal structure and orientation of each grain, diffraction patterns, similar to Kikuchi patterns in TEM, are produced from these forward scattered electrons. These electrons are detected using a phosphor screen interfaced with a Charged Coupled Device (CCD) camera.

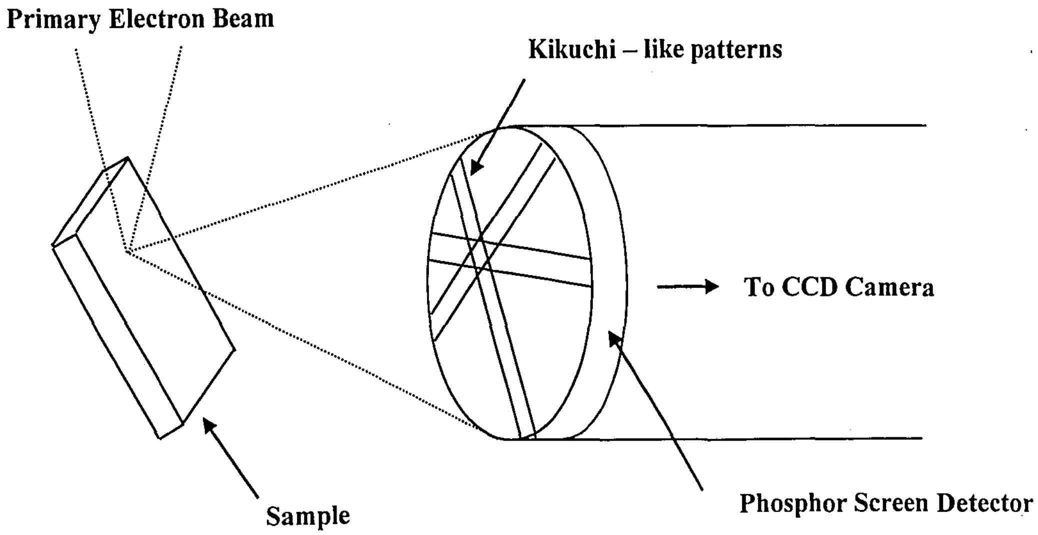

Figure 9: Schematic diagram showing the setup of the EBSD system in an SEM chamber.

A schematic diagram showing the setup of the EBSD system in an SEM is shown in Figure 9. An example of the indexing capability is shown in Figure 10. On the left is the Kikuchi – like pattern overlaid with the indexing for a generic FCC material. On the right, the software has identified the material to be most likely FCC material. The good spatial resolution allows grains less than 1 μm in size to be examined.[18] The advantage of EBSD over previous orientation determination techniques, such as transmission electron microscopy and powder diffraction, is that it can determine the orientation for many individual grains from a relatively bulky sample. Also, the EBSD technique requires more traditional sample preparation and is not an average orientation determined from many grains. The software developed also controls the electron beam of the microscope to map the diffraction patterns of a certain area of the sample. In this manner, for a given material, the relationship between the morphology of many grains and its crystallographic orientation can be made. In the case of hot deformed aluminum, the microtexture, or preferred orientation of specific grains in the microstructure, can be determined. As a result of imparting strain on a crystal, the orientation of these grains changes to a preferred orientation that is not random. In FCC crystals, for example, the texture due to rolling has been identified as being a mixture of three ideal textures, (110)[-112], (112)[11-1], and (123)[1-21].[3] In extrusion, the orientation changes that take place are much more complex than that in more symmetrical deformation processes such as drawing and rolling. In extrusion, there are zones of deformation where there are variations in strain, strain rate and temperature.

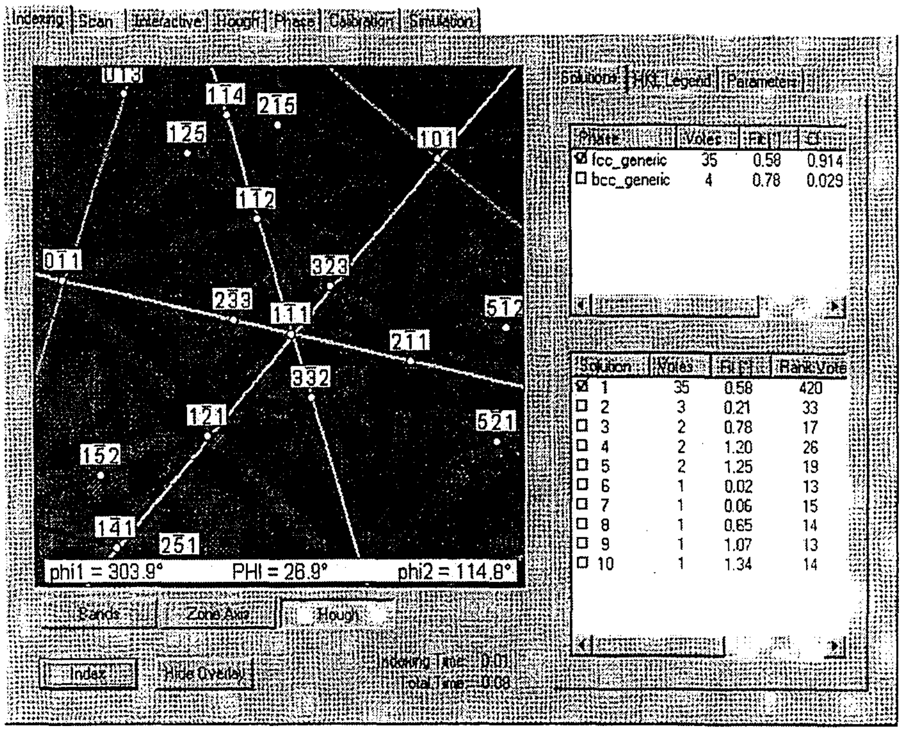

Figure 10: Representation of indexing capabilities of the TSL EBSD software. On the left are Kikuchi – like lines that are overlaid with the indexing from the software. The software has identified the pattern as FCC generic.[19]

Texture is dependent upon all of these parameters, and therefore the texture at the center of an extrudate could be completely different than that at the surface. This is because the center of an extrudate may undergo different deformation than the surface. EBSD has been performed in the past on a partially extruded 6105 alloy billet in order to determine the orientation changes which take place during deformation.[11] It was found that the grains rotate in certain zones of deformation to accommodate for the strain being imparted on them. In FCC metals like aluminum, slip is the dominating deformation mode.[20] Several theories on the relationship between texture and plasticity have been developed. The most recognized full constraints model by Taylor, predicts a rotation towards the <111> or <100> orientation for FCC metals. A <100> fiber deformation texture has been reported after axisymmetric compression, while a mixture of <111> and <100> are seen in extruded aluminum rods.[21] The texture of a material has very important influences on a material's mechanical properties such as strength and ductility. In addition, it has been found that after post – deformation annealing, the recrystallization texture will be influenced by the deformation texture.[20]

2.0 EXPERIMENTAL PROCEDURE

2.1 Billet Material

The aluminum alloys used in this research include 6061 and 6063. DC cast 6063 material was supplied by Easco Aluminum. The 6061 material was sectioned from the mid – radius of a 20.32 cm (8 in.) homogenized billet from Werner Co. Variations in the chemistry and structure of a cast billet occur due to the casting process. Therefore, the mid-radius of a billet is used as a location for samples for simulation because it is most representative of the material and is most free from inhomogeneities. The 6063 samples were sectioned from a 17.78 cm (7 in.) homogenized billet from Ormet Corp. This billet was homogenized at 560^0 C (1040^0F) for 4 hrs. and quenched at a rate of greater than 200 ^{0}C/min. (392 ^{0}F/min.). The sections from the each billet were then machined to 10 mm diameter Gleeble samples, 120 mm in total length for thermal simulation with 15 mm length threads. Compression samples were 90 mm in length with no threaded areas. The ends of the thermal simulation samples were threaded and could then be used as tensile samples to test the results of heat treatment.

2.2 Gleeble Simulation

2.2.1 Equipment Setup and Procedure

The Gleeble thermal – mechanical simulator was originally designed for testing steel samples, but has been altered to accommodate the analysis of other materials. Because of the relatively high thermal conductivity of aluminum, stainless steel jaws must be used instead of the traditional copper jaws that are used for steel samples. An example of a typical thermal cycle setup is shown in Figure 11. Thermocouples are placed at the center of the sample between the jaw faces in order to provide temperature control. Heating rates of over 1,000 ^{0}C / s are capable using this equipment. In addition, the Gleeble has the capability to perform controlled cooling rates using a quench spray head that can impinge water, air, or a combination of both on the sample in the enclosed chamber. To control the heating and cooling rate, the Gleeble automatically adjusts the current input based on the program temperature and thermocouple reading. These jaws are water cooled, which create a "work – zone" in the center of the sample. A temperature gradient exists in the free span between the jaws, both radial and longitudinal (see Figure 12). Much work was performed to determine the size of this work zone because this is the area where constant temperature, and therefore, constant microstructure, exists. Stainless steel "hot – jaws" were used in thermal cycle simulation for the aluminum alloys because of its lower thermal conductivity over copper.

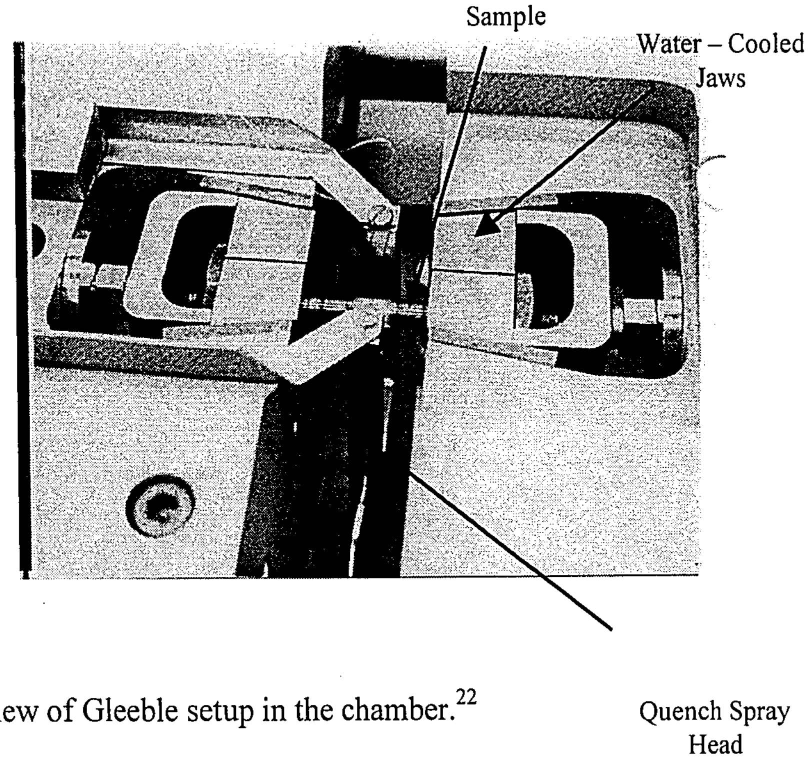

Figure 11: View of Gleeble setup in the chamber.[22]

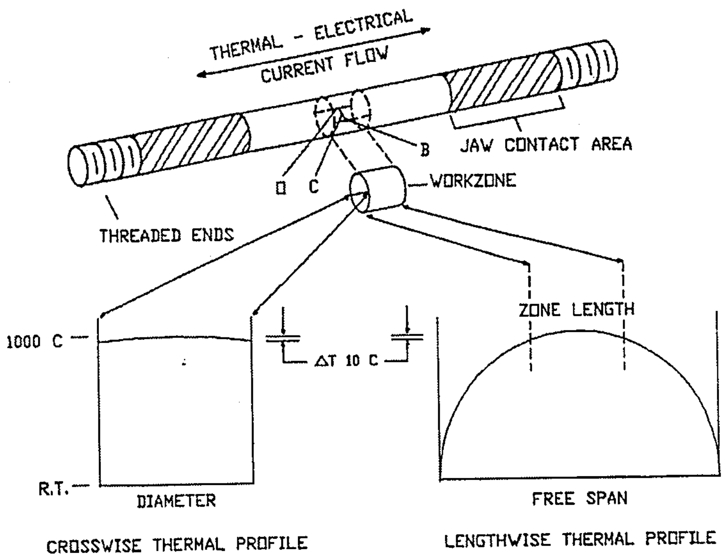

Figure 12: Schematic diagram showing the thermal gradient in Gleeble sample due to water cooled jaws.[22]

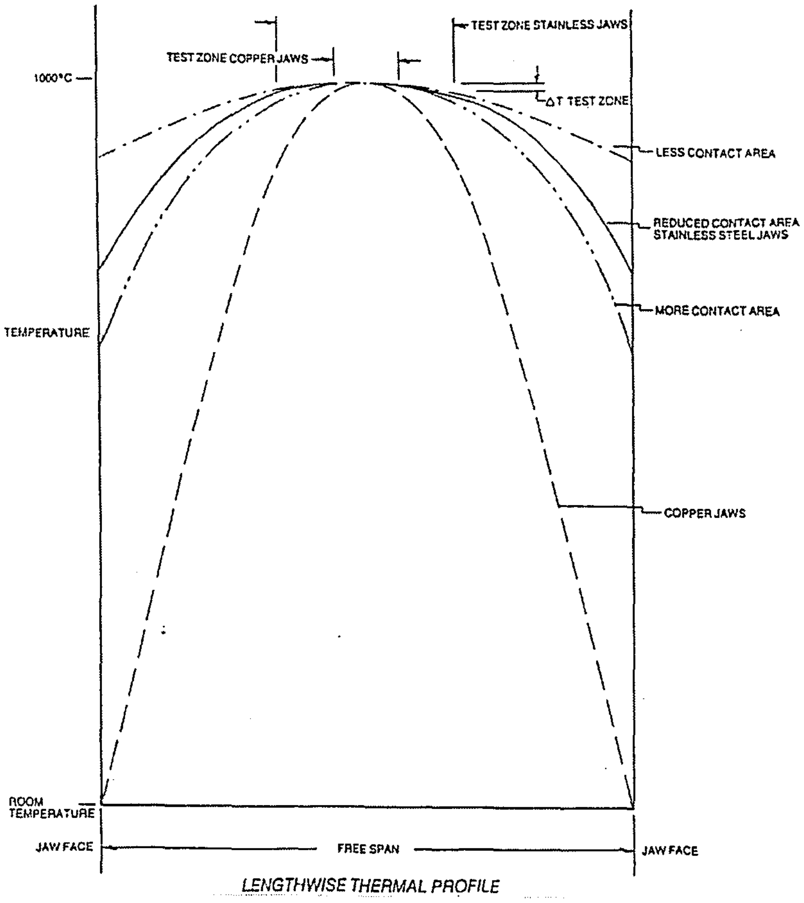

Figure 13: Thermal gradients due to water – cooled stainless steel jaws and copper jaws.[22]

These jaws have a recessed contact area that increases the work zone size as can be seen in Figure 13. In addition to accurate heating, the Gleeble is capable of accurate high quench rates with the use of a quench spray head. This spray head lies in the middle of the work zone, as seen in Figure 11.

2.2.2 Thermal Cycles

A matrix of thermal cycle profiles was created in order to determine the effect of varying the temperature on the resultant microstructure and mechanical properties of the sample. The thermal profiles representing billet heating, deformation heating, and press quenching were produced which resemble typical times and temperatures seen in industrial extrusion practice. Depending on the alloy, different preheating and extrusion temperatures, as well as cooling rates, are used. For example, since 6061 contains more Mg and Si, the melting point of the alloy is reduced. Therefore, the maximum allowable extrusion temperature will be lower than for a 6063 alloy. Also, because 6061 is more highly alloyed, it is more quench sensitive and requires a faster post extrusion cooling rate and a longer preheat time.

Thermal cycle profiles for a 6061 alloy are shown in Figure 14 (A-D). The preheat thermal profile represents heating from a gas fired furnace, where a maximum and minimum temperature were assumed to be 510 ^{0}C (950 ^{0}F) and 454 ^{0}C (850 ^{0}F) respectively. Between billet preheating and extrusion the temperature is lowered due to transfer of the billet between the preheat chamber and the extrusion chamber. Temperature rises during extrusion between 75 ^{0}C (167 ^{0}F) and 100 ^{0}C (212 ^{0}F) have been reported.[23] The maximum extrusion temperature was selected to be the temperature of the extrudate as it exits the die, where a maximum was assumed to be 551.7 ^{0}C (1025^0 F) and a minimum to be 523.9 ^{0}C (975^{0}F). In addition, samples were run through only the low and high preheat cycle. Post extrusion cooling rates were

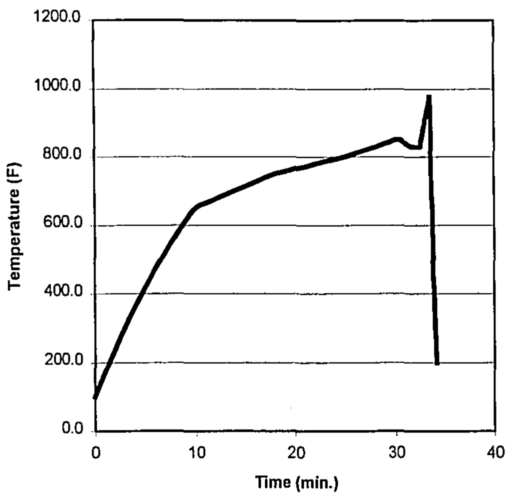

A) Low Preheat – Low Extrusion Temperature

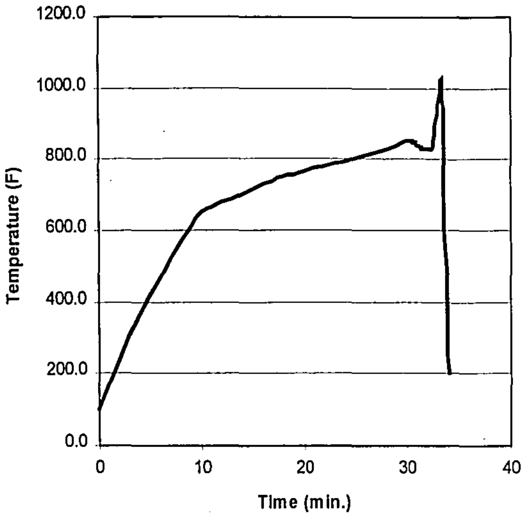

B) Low Preheat – High Extrusion Temperature

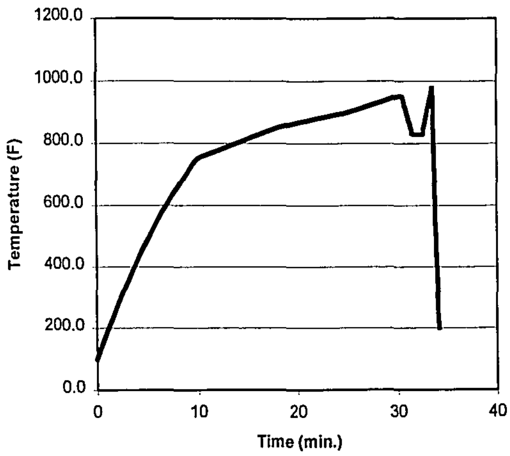

C) High Preheat – Low Extrusion Temperature

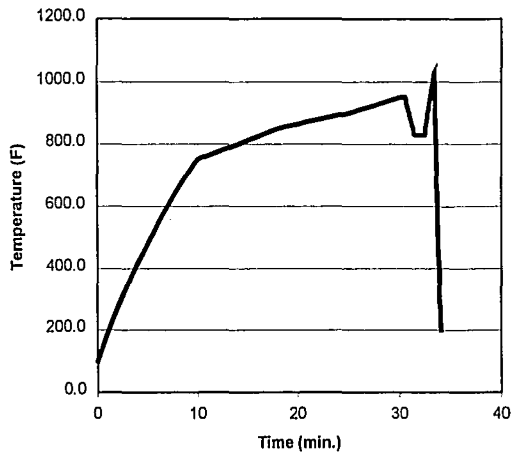

D) High Preheat – High Extrusion Temperature

Figure 14 (A-D). Thermal cycle profiles for 6061 using Gleeble simulation equipment. The preheat times are representative of profiles from a gas fired furnace. The maximum deformation temperatures are based on the extrudate exit temperature.

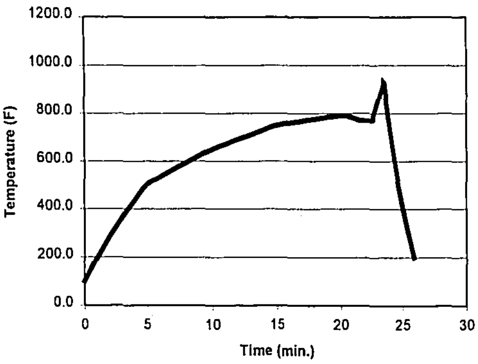

A.) Low Preheat – Low Extrusion Temperature

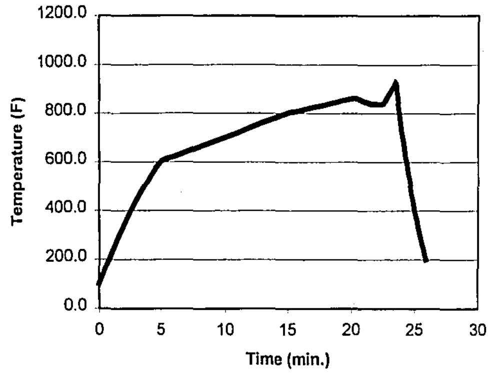

B.) High Preheat – Low Extrusion Temperature

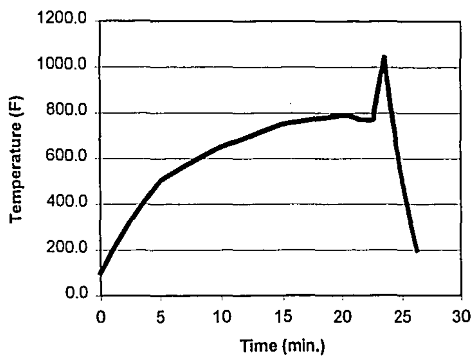

C.) Low Preheat – High Extrusion Temperature

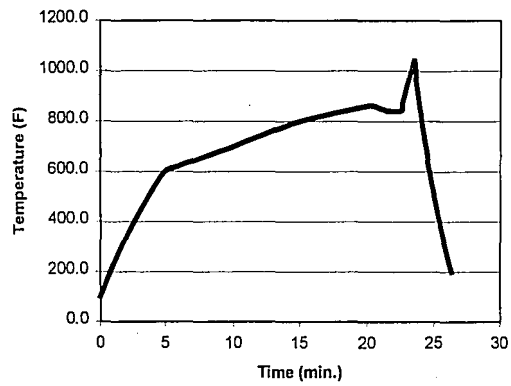

D.) High Preheat – High Extrusion Temperature

Figure 15 (A-D): Thermal cycle profiles for 6063 simulation. The preheat times are representative of profiles from a gas fired furnace. The maximum deformation temperatures are based on the extrudate exit temperature.

performed at 704.4 ^{0}C/min. (1300^0 F/min). Samples were subsequently aged in a laboratory furnace for 6 hrs. at 176 ^{0}C (350 ^{0}F).

The different thermal cycles used for 6063 alloy are shown in Figure 15 (A-D). The billet preheating temperatures simulated resemble those from a gas – fired furnace. High and low preheat temperatures of 460^0 C (860^0 F) and 410^0 C (770^0 F) were used. Extrusion temperatures were based on the exit temperature of extrudates as they exit the die. A maximum of 560^0 C (1040^0 F) and a minimum of 496^0 C (925^0 F) were used. Post deformation cooling rates of 149^0 C/min (300^0 F/min.) were used. In addition to these thermal cycles, samples were run only through either the low or high preheat thermal cycle and quenched to determine to the effect on microstructure without deformation heating. Samples were subsequently aged for 6 hrs. at 176 ^{0}C (350 ^{0}F).

2.3 Mechanical Property Determination

Tensile testing was performed on samples that were run through each of the thermal cycles. Samples were machined with reduced gauge sections after the samples were run in the Gleeble. In order to limit the size of the work zone as the representative area being tested, shortened gauge lengths were used. The dimensions of the sample were 0.64 cm (0.25 in.) reduced diameter and 1.91 cm (0.75 in) gauge length. Superficial N – 15 hardness testing was also performed on the aged samples.

2.4 Compression Testing Setup

The setup for hot compression testing is similar to that in the thermal cycle procedure, except that the samples are not threaded, and the free span is much smaller. Ideally, the length to diameter ratio for Gleeble compression testing should be less than 3 in order to avoid buckling. Uniaxial compression testing was performed using a Gleeble 1000 HAZ thermal – mechanical simulator. Compression temperatures used were 400 (752), 500 (932), and 600 (1112) ^{0}C (^{0}F). The samples were subsequently quenched immediately after deformation in order to preserve the microstructure. Ram speed was varied between .1 and .2 cm s^{-1} and strains of 0.1, 1, and 1.5 were performed. True compressive strain was calculated using the following equation[1].

$$\varepsilon_c = \ln h_0 / h$$

where:

ε_c – true compressive strain

h_0 – original height

h – final height

2.5 Electron Backscatter Diffraction

2.5.1 Equipment Setup and Procedure

Electron Backscatter Diffraction (EBSD) analysis was performed using a Philips Electroscan Environmental SEM and EBSD equipment made by TexSEM Laboratories (TSL). Samples used in compression testing were sectioned parallel to the axis of compression. The samples were subsequently mechanically ground and polished carefully to the exact mid – thickness of the samples. However, a thin deformation layer from preparation still exists after this procedure. Therefore, a short etch was performed immediately prior to EBSD analysis using a 10% HF aqueous solution to remove any oxide and deformation layer. The actual texture of the material should not be severely affected by this procedure. If any change in structure is associated with preparation, one effect may be scattered crystallographic data presented in the pole figure. One way to improve pattern quality would be to use electropolishing techniques. Any deformation layer created during mechanical preparation is therefore not an issue.

The TSL software automatically produces grain maps and resulting pole figures based on diffraction patterns generated. Diffraction patterns are indexed using a Hough transform, which essentially finds the highest intensity diffraction pattern that strikes the phosphor screen. Maps can be generated which display image quality (quality of the diffraction pattern), texture, and discrete grains. Texture maps were generated from each of the three different zones of deformation in compression samples. Inverse pole figures were generated based on these maps. An inverse pole figure displays information on the relative grain orientation with respect to the sample axes. Sample preparation proved to be an important factor in obtaining worthwhile data, because of the inherent difficulties with deformed aluminum. Aluminum's low atomic number coupled with the dislocation density increase in a deformed material, hampers pattern quality. Performing a stress relief anneal to decrease the dislocation density may improve pattern quality, but was not deemed necessary in this experiment. Electropolishing could also be used to improve pattern quality because no deformation is introduced during surface preparation.

2.5.2 Inverse Pole Figures

The information gained from EBSD analysis can be presented in many ways. A traditional method of presenting texture information has been with pole figures. A pole figure is a stereographic projection that is viewed from the top of a sphere down to the equator. Another method to represent the data is in an inverse pole figure. An inverse pole figure is similar to the traditional pole figure except that it takes into account the reference directions that texture is being measured in. For example, in compression testing, the 100 direction was considered the axis of compression. If a strong texture were present in that direction, contour lines would build up in that corner of the inverse pole figure. A schematic diagram showing the relationship between crystal and specimen axes is shown in Figure 16. Inverse pole figures are created for three different directions. These figures are plots of the frequency with which a specific direction coincides with one of the specimen axes. In this case, the compression direction is the [100], the sample normal is the [001], and the transverse direction is [010]. Figure 16 shows this relationship between the sample orientation and the crystal orientation (a_1^c, a_2^c, a_3^c). Knowing angles between sample directions and crystallographic directions allows one to describe the relationship between processing and crystallographic directions.

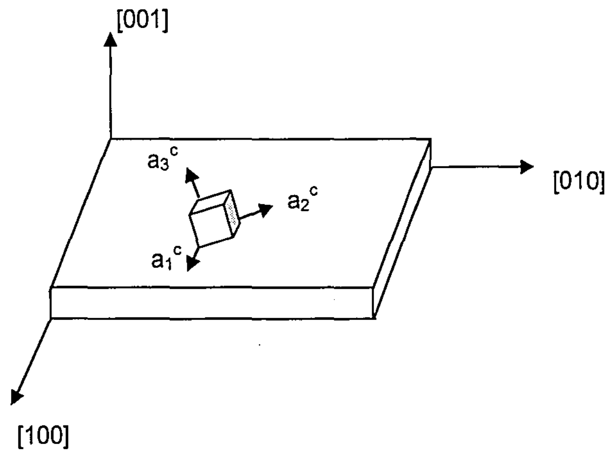

Figure 16: Schematic representation of the relationship between crystallographic and specimen axes.

3.0 RESULTS

3.1 Casting and Homogenization Microstructures

Sample material for Gleeble simulation included as – cast 6063 alloy, homogenized 6063 and homogenized 6061 alloy. As was previously stated, it is important that all stages of the extrusion process be taken into account in order to determine the influence of processing parameters. In this case, the condition of the material before simulation occurs is kept constant. The simulation is limited to processes after homogenization. All material was characterized by either Light Optical Micrographs (LOM) or SEM images. The as – cast microstructure of 6063 is shown in Figure 17. Notice the brittle α AlFeSi phase. The as – received homogenized 6061 microstructure is shown in Figure 18. The homogenized 6063 alloy is shown in Figure 19.

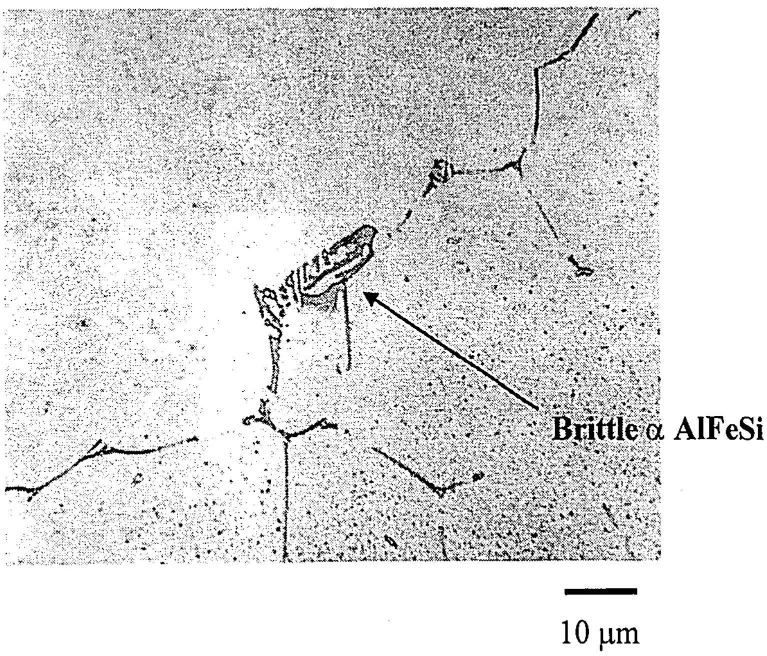

Figure 17: LOM – As – cast microstructure of 6063 aluminum alloy. (Keller's etch)

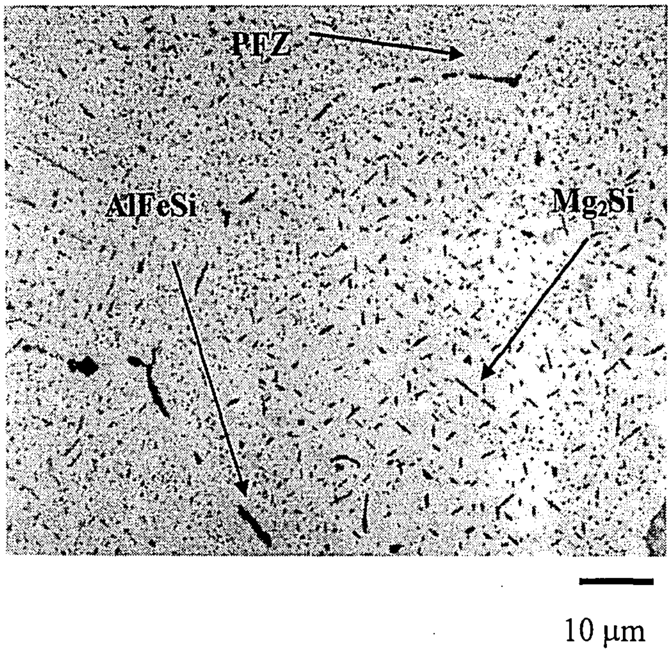

Figure 18: LOM - Original homogenized 6061 microstructure before extrusion thermal cycle. (Keller's etch)

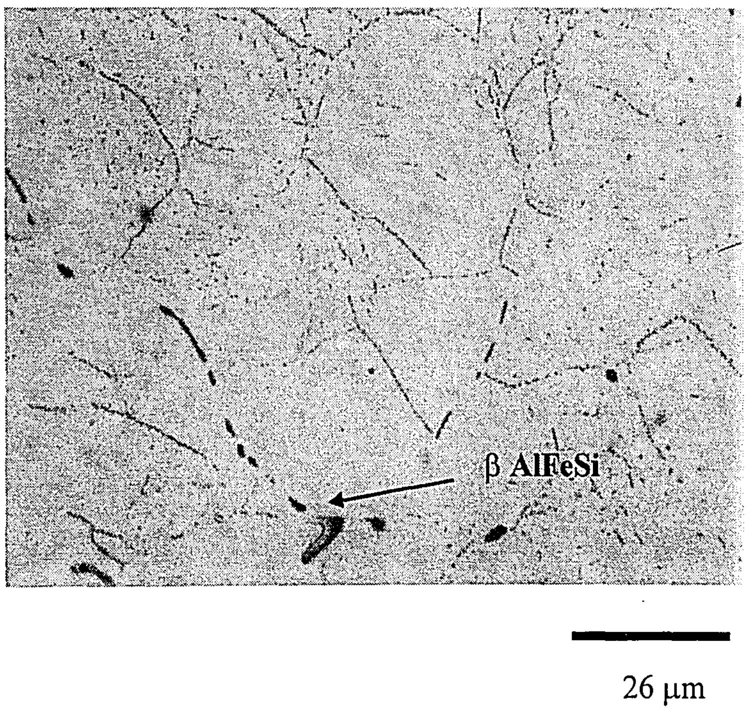

Figure 19: LOM – Homogenized 6063 microstructure. Notice diminished amounts of Mg_2Si precipitates over the 6061 alloy. (Keller's etch)

3.2 Thermal Cycle Simulation Microstructures

Thermal cycles were performed on the Gleeble to simulate the extrusion process from preheating the billet to ageing. In order to determine the microstructure of the billet just before extrusion takes place, samples were run through the preheat thermal cycle and then water quenched to room temperature just before the extrusion thermal cycle step. The remaining samples were run through the full thermal cycles and then aged.

3.2.1 6061 Alloy Microstructures

The 6061 alloy samples that were run through the high and low preheat temperatures only are shown in Figures 20 and 21. It can be seen that the high preheat sample has considerably less Mg_2Si still precipitated than the low preheat. In addition, the Mg_2Si is also much smaller and more rounded in the high preheat sample.

The microstructures from the high and low preheat and extrusion thermal cycles of 6061 are shown in Figures 22 through 25. The figures reveal that as the preheat and extrusion temperatures were increased, the amount of Mg_2Si that goes into solution increases. The time allowed for this to occur remained constant in all thermal cycle cases. Samples were also run through these same thermal cycles and then subsequently aged in the T6 heat treatment. The results of these microstructures are seen in Figures 26 and 27 for 6061 alloy.

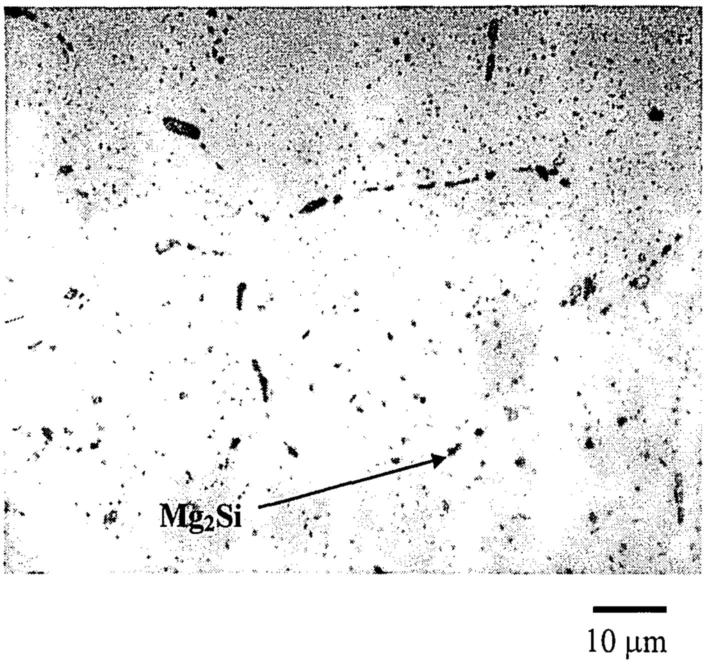

Figure 20: LOM – 6061 microstructure frozen just after high temperature preheat. (Keller's etch)

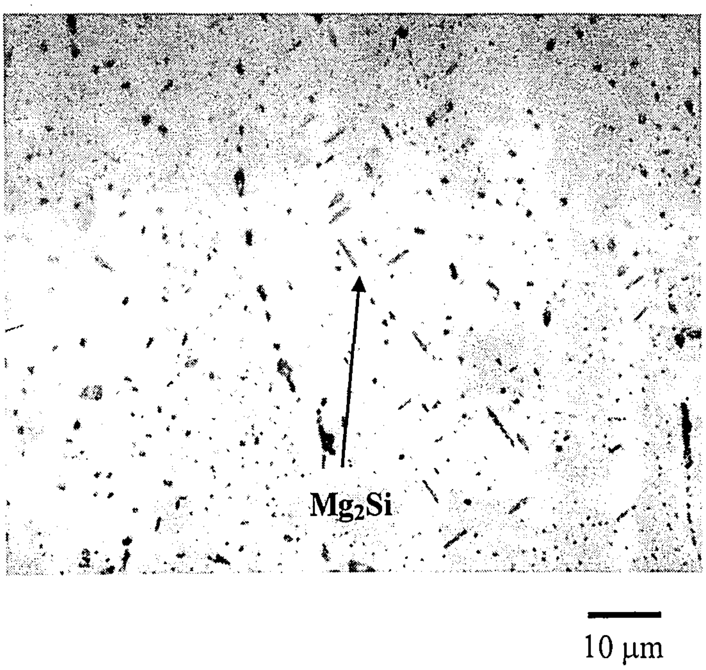

Figure 21: LOM – 6061 Microstructure frozen just after the low temperature preheat cycle showing coarse Mg_2Si precipitates. (Keller's etch)

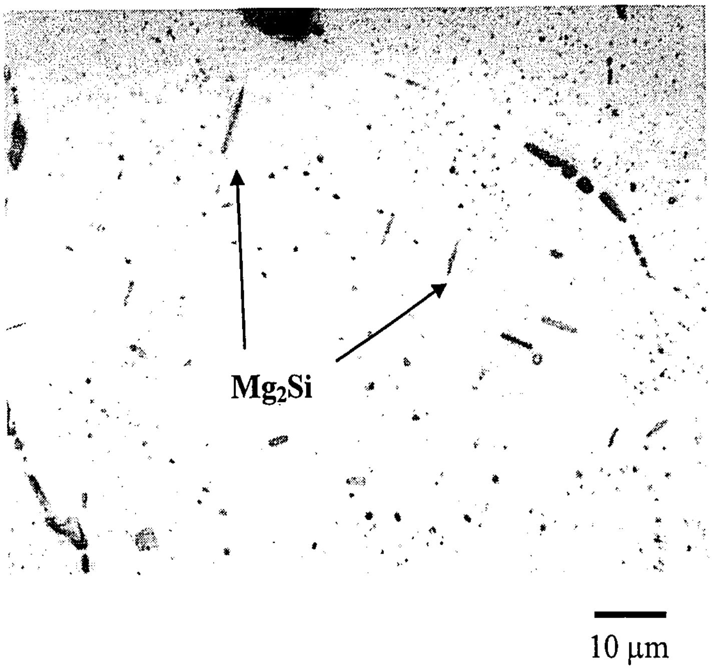

Figure 22: LOM – 6061 low preheat, low extrusion temperature with retained coarse Mg_2Si. (Keller's etch)

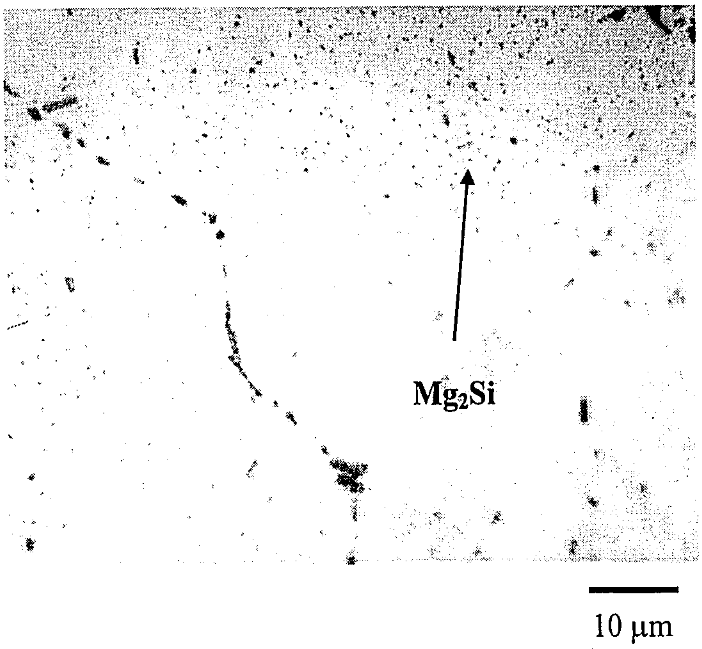

Figure 23: LOM – 6061 high preheat, low extrusion temperature microstructure. (Keller's etch)

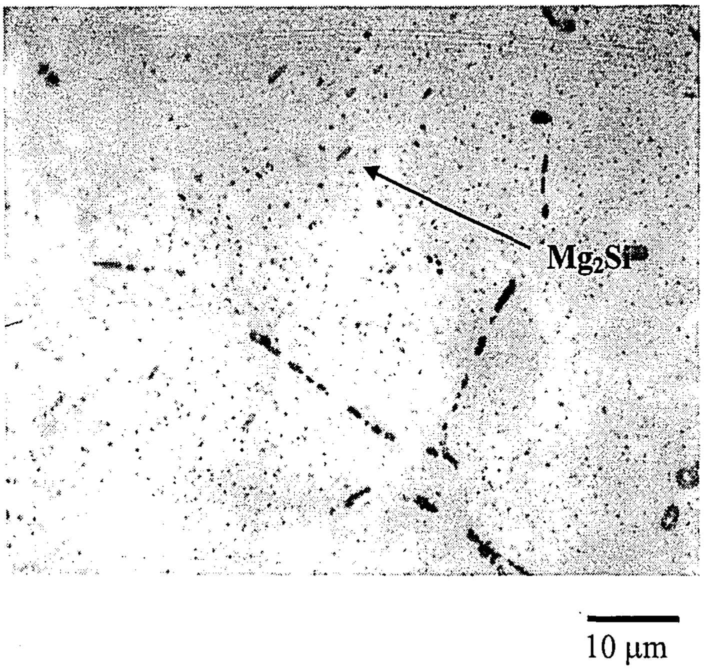

Figure 24: LOM – 6061 low preheat, high extrusion temperature microstructure. (Keller's etch)

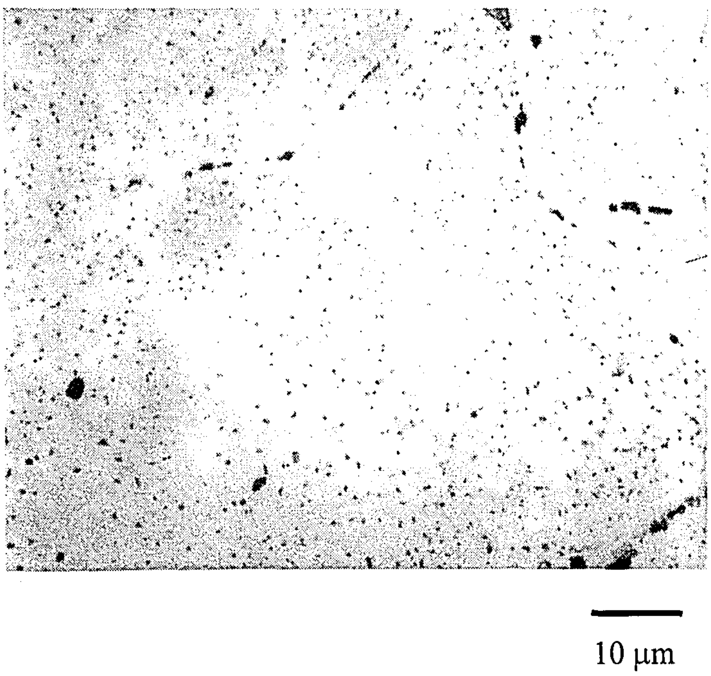

Figure 25: LOM – 6061 high preheat, high extrusion temperature with most solutionized structure. (Keller's etch)

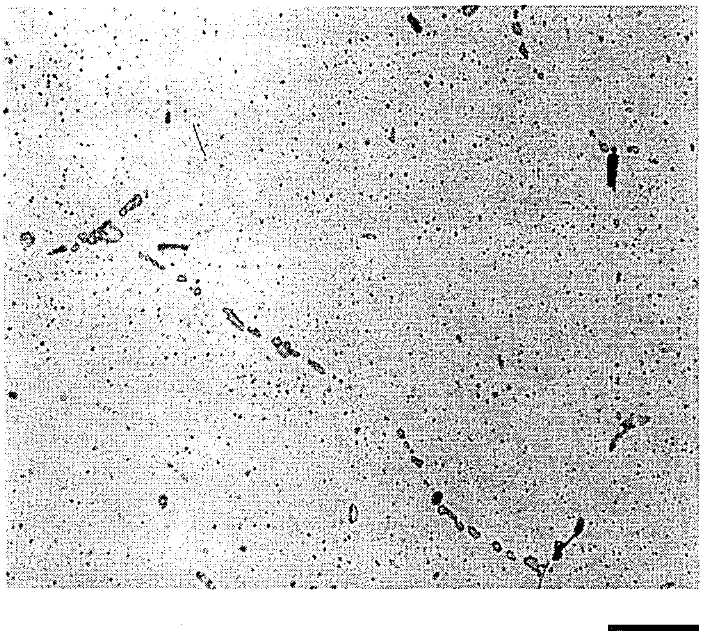

Figure 26: LOM – 6061 alloy after high preheat and high extrusion thermal cycle and aged in T6 condition at 350^0F for 6 hours with finely dispersed precipitates. (Keller's etch)

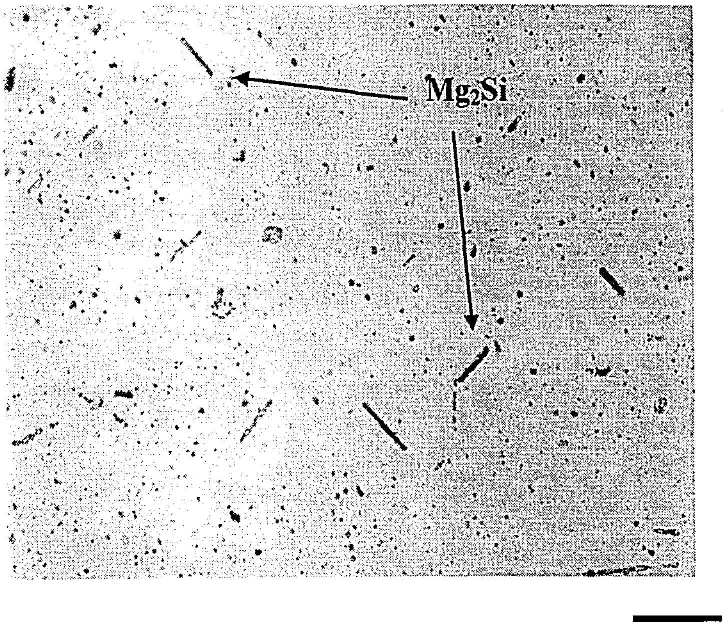

Figure 27: LOM - 6061 alloy after low preheat and low extrusion thermal cycle and aged in T6 condition at 350^0F for 6 hours. (Keller's etch)

3.2.2 6063 Alloy Microstructures

Samples of homogenized 6063 alloy were run through low and high preheat cycles and subsequently quenched to room temperature to preserve the microstructure. The resultant microstructures are shown in Figures 28 and 29. Samples were then run through the high and low preheat and extrusion temperature cycles and air – quenched after extrusion. The resultant microstructures after these combinations of thermal cycles are shown in Figures 30 through 33. It was again determined that the higher preheat and extrusion temperatures yielded the more solutionized structure. Samples underwent post extrusion ageing in the T6 temper at 177^{0}C (350^{0}F) for 6 hrs. The resultant microstructures of these aged samples is shown in Figures 34 and 35.

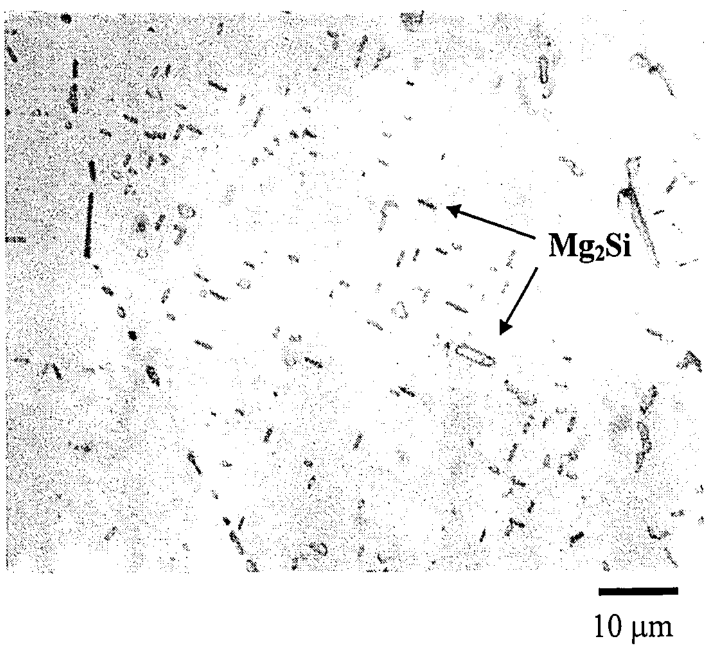

Figure 28: LOM – 6063 microstructure after low preheat temperature only. (Keller's etch)

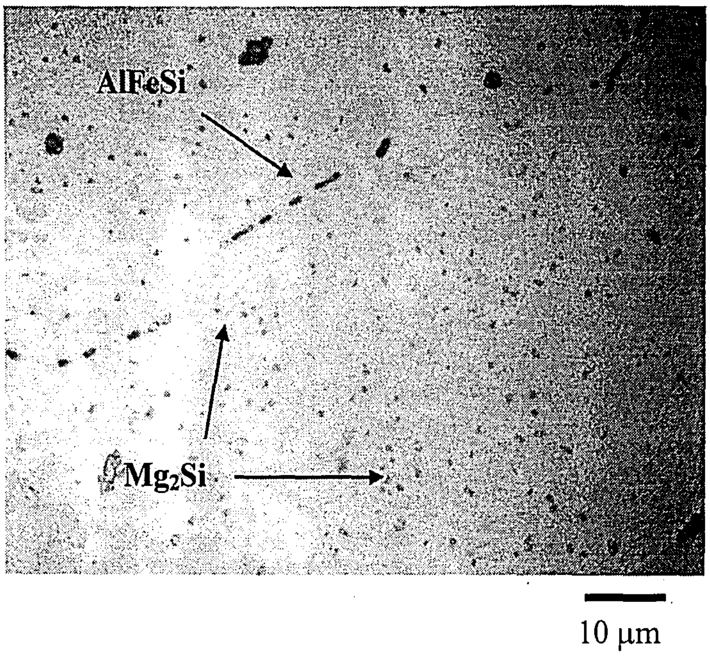

Figure 29: LOM – 6063 microstructure after high temperature preheat only. (Keller's etch)

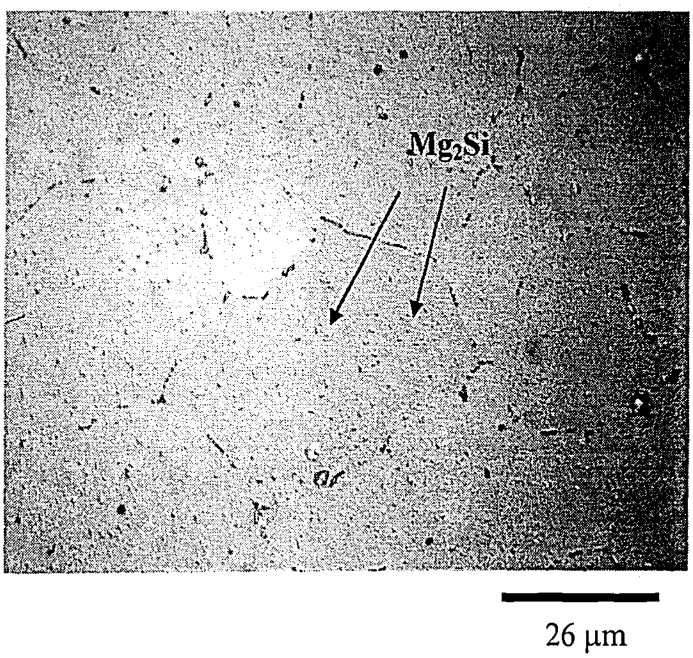

Figure 30: LOM – 6063 microstructure after low preheat temperature and low extrusion thermal cycle. (Keller's etch)

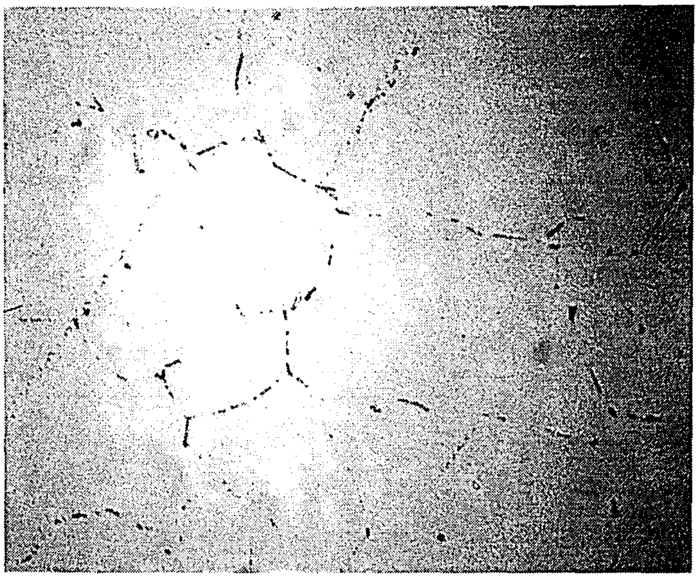

26 μm

Figure 31: LOM – 6063 microstructure after low temperature preheat and high extrusion thermal cycle. (Keller's etch)

26 μm

Figure 32: LOM – 6063 microstructure after high preheat temperature and low extrusion thermal cycle. (Keller's etch)

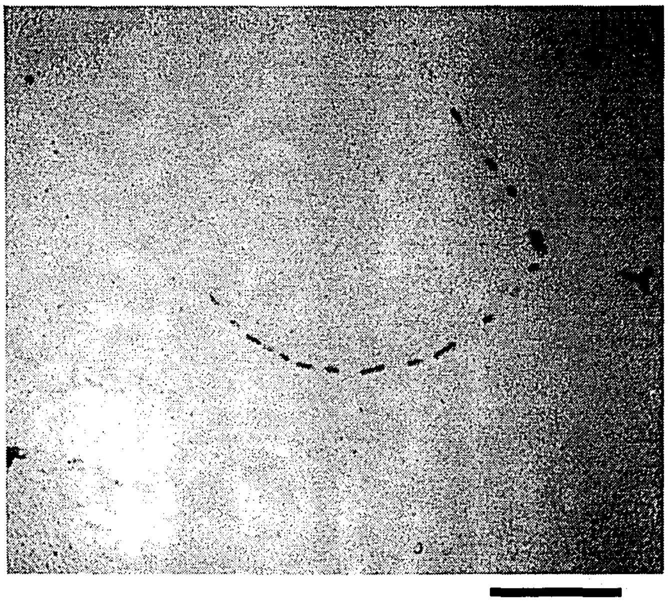

10 μm

Figure 33: LOM – 6063 microstructure after high preheat temperature and high extrusion thermal cycle. (Keller's etch)

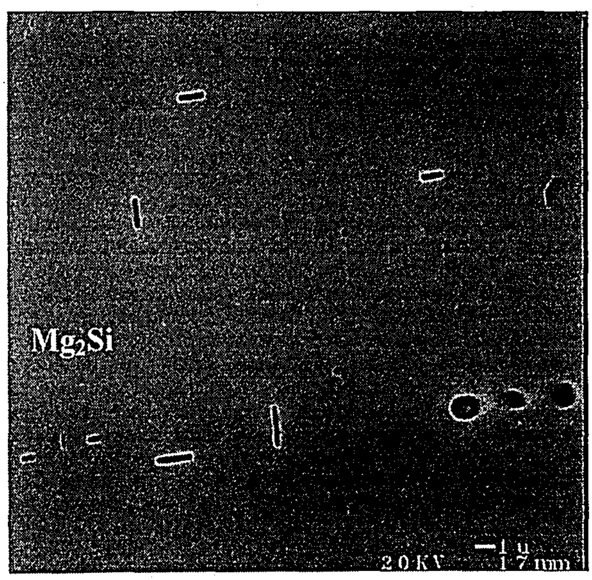

Figure 34: SEM image of 6063 alloy after low preheat and low extrusion thermal cycle and aged in T6 condition at 350^0F for 6 hours. Notice coarse Mg_2Si present in the structure.

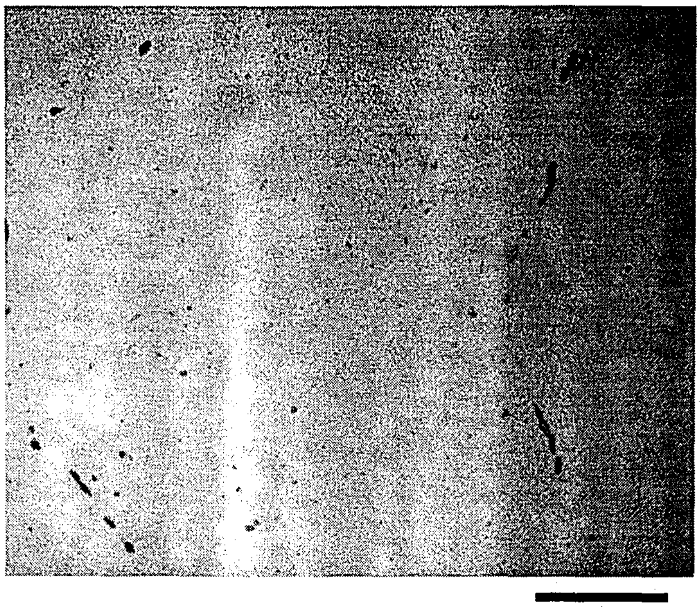

10 μm

Figure 35: 6063 alloy after high preheat temperature and high extrusion thermal cycle and aged in T6 condition at 350^0F for 6 hours. (Keller's etch)

3.3 Mechanical Property Results

Tensile testing was performed on samples that underwent extrusion simulation. Each combination of low and high preheat and extrusion temperatures was tested. The results are shown in Tables III and IV. The results show that the high preheat and extrusion temperatures had higher levels of solid solution hardening and mechanical properties were slightly increased. Superficial N –15 hardness measurements were performed on samples that had underwent extrusion simulation followed by ageing and are shown in Table V.

Table III: Mechanical property data from naturally aged 6061 simulation samples.

Extrusion Thermal Cycle	**UTS ksi**	**YS ksi**	**Elong. %**
High Preheat – High Extrusion	36.5	16.0	33.6
High Preheat – Low Extrusion	35.3	14.8	34.6
Low Preheat – High Extrusion	33.8	14.4	36
Low Preheat – Low Extrusion	32.0	13.4	40

Table IV: Mechanical property data from naturally aged 6063 simulation samples.

Extrusion Thermal Cycle	**UTS (ksi)**	**YS (ksi)**	**Elong. %**
High Preheat – High Extrusion	25.3	12.4	43
High Preheat – Low Extrusion	25.0	11.3	45
Low Preheat – High Extrusion	24.8	10.7	46
Low Preheat – Low Extrusion	22.5	10.0	49

Table V: Hardness Data from 6061 and 6063 alloy aged at 177^{0}C (350^{0}F) for 6 hours.

Alloy and Temper	**HR N - 15**
6061 Low Preheat / Low Extrusion + T6 Age	113.0
6061 High Preheat / High Extrusion + T6 Age	95.0
6063 Low Preheat / Low Extrusion + T6 Age	49.5
6063 High Preheat / High Extrusion + T6 Age	68.5

The samples that underwent low preheat and low extrusion cycles and aged had lowest hardness values. High preheat and high extrusion thermal cycle samples showed the highest hardness values after ageing for both alloys.

3.4 Compression Testing Results

Figure 36 shows compression samples reduced to 20%, 40%, and 60% of their original size. Barreling was observed and it increased with increasing strain. Samples were carefully ground and polished to the exact mid – thickness of the sample. In Figure 37 the macroetched cross – section of the sample reveals the area consistent with Zone I, resembling a dead metal zone in extrusion.

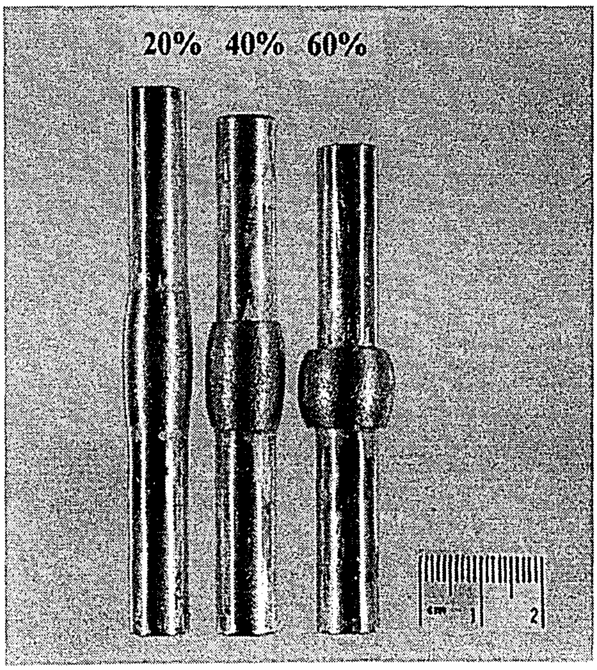

Figure 36: Compression samples reduced to 20%, 40%, and 60% of original height.

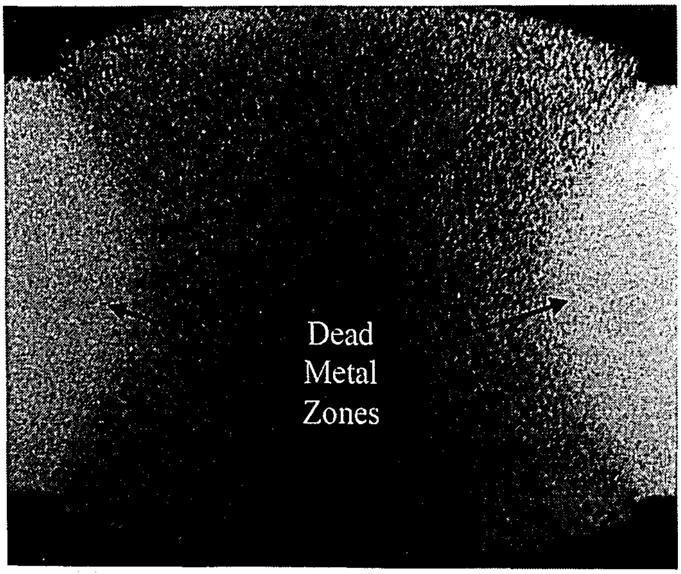

Figure 37: Image of macroetched compression sample showing area resembling dead metal zone in extrusion.

A closer inspection of the Zone I microstructure is shown in Figure 38, and reveals its equiaxed structure. The interface between Zone I and Zone II revealed macroscopic slip bands consistent with low levels of strain (Figures 39 and 40). It should be noted that these macroscopic slip bands are revealed by multiple slip on several adjacent planes.

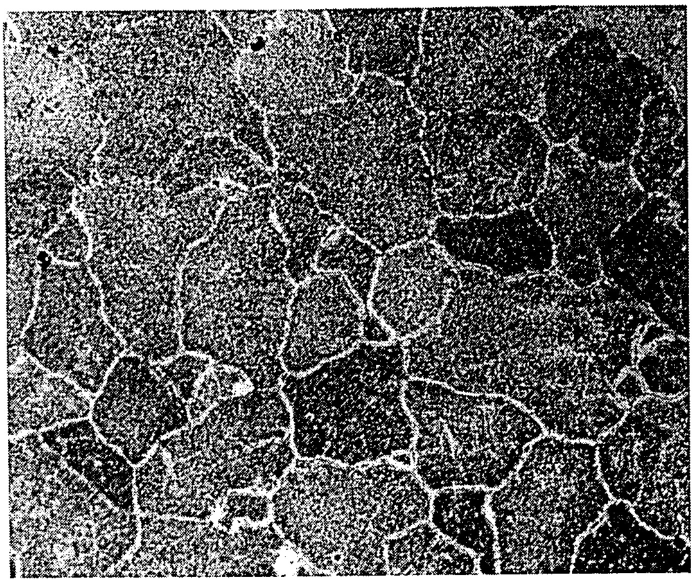

60 µm

Figure 38: Microstructure from Zone I of the compression sample. (5% HF)

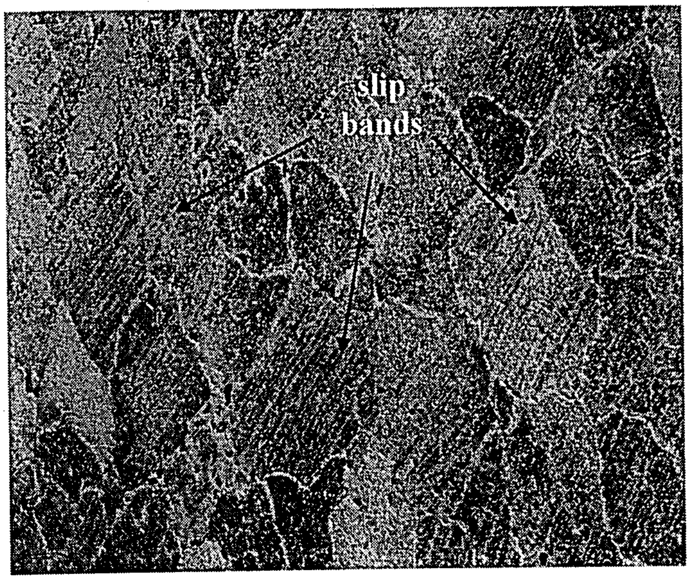

60 µm

Figure 39: LOM image of interface between Zone I and Zone II. Notice slip bands in certain grains. (5% HF)

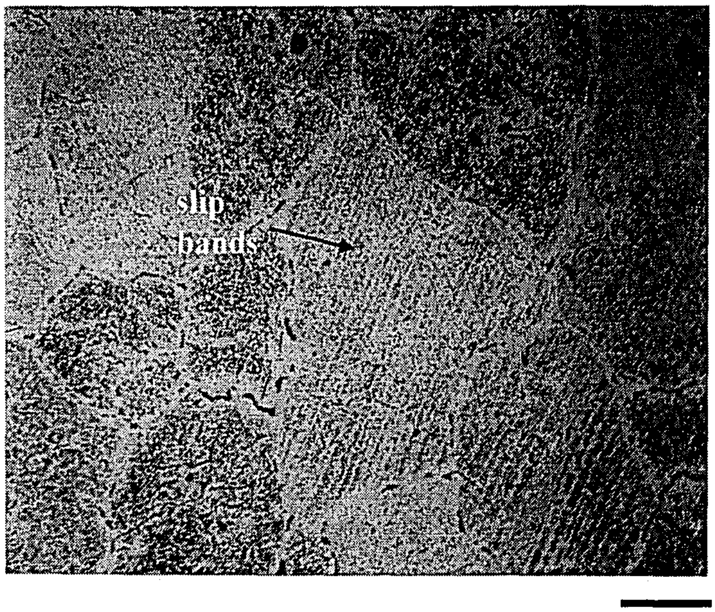

Figure 40: Magnified LOM image of slip bands in certain grains at the interface between Zone I and Zone II. (5% HF)

Figure 41 shows the microstructure of the area corresponding to the area of Zone II of the compression sample. The grains appear to be deformed laterally perpendicular to the axis of compression. Figure 42 shows the microstructure corresponding to the area of Zone III. Texture determination was performed on all three zones of the sample. The inverse pole figure from Zone I representing the dead metal zone of a partially extruded billet can be seen in Figure 43. The relative strength of texture, if there is any present, can be determined by the strength of the intensity contour in the legend at the bottom right. In Figure 44, inverse pole figures are shown for Zone II of the compression sample. It can be seen that a majority of grains are oriented close to the <110> family of crystallographic directions along the compression axis. Figure 45 shows inverse pole figures from Zone III of the compression sample. A tendency towards the <111> family of directions is revealed in the direction of compression.

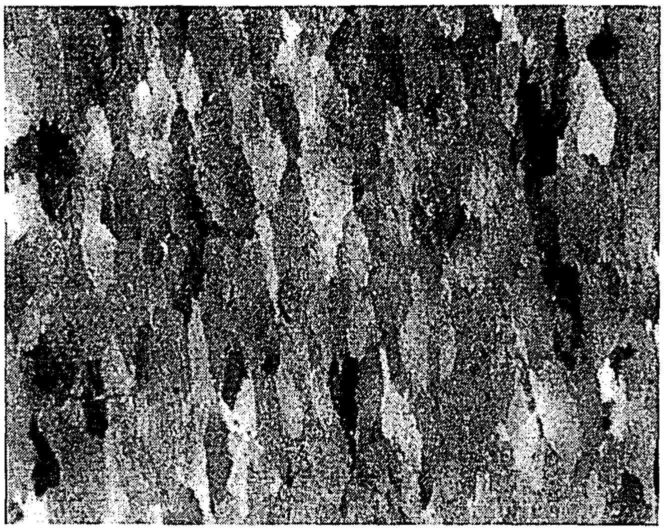

100 μm

Figure 41: LOM image under polarized light of the deformed grains from Zone II of the compression sample.

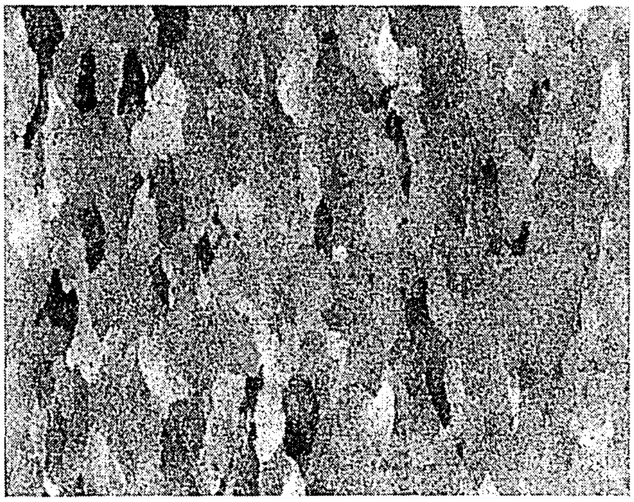

100 μm

Figure 42: LOM image under polarized light of the deformed grains from Zone III of the compression sample.

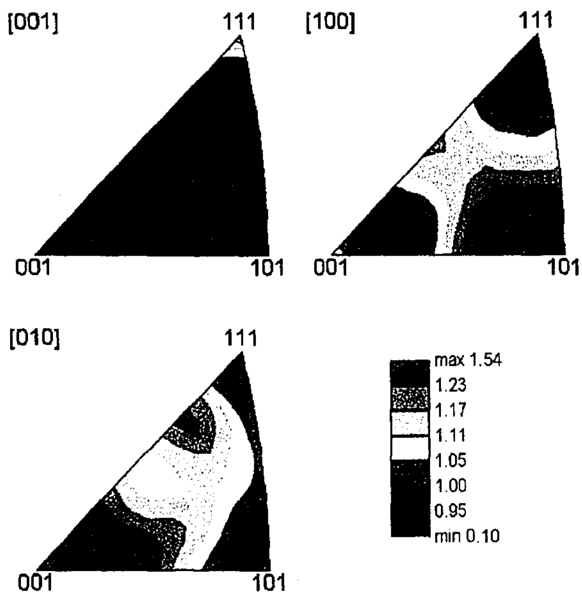

Figure 43: Inverse pole figure produced from EBSD on undeformed region of Zone I in the compression sample.

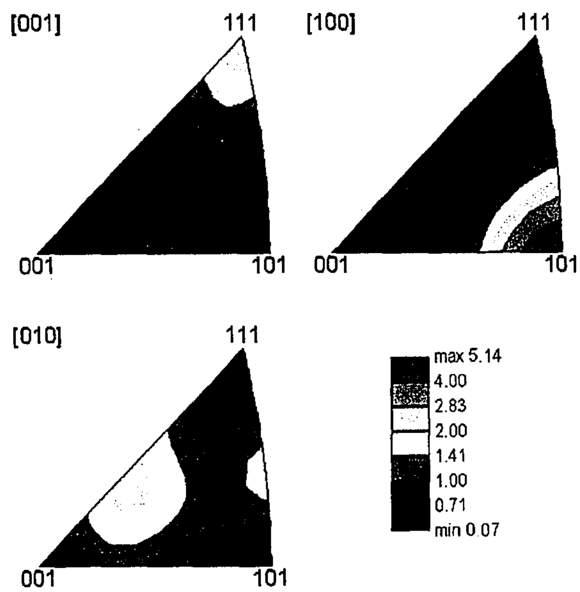

Figure 44: Inverse pole figure produced from EBSD on undeformed region of Zone II in the compression sample.

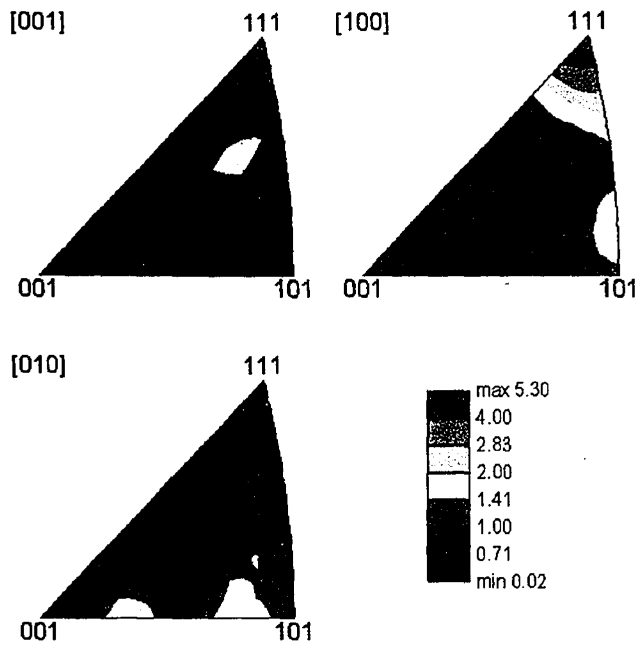

Figure 45: Inverse pole figure produced from EBSD on undeformed region of Zone III in the compression sample.

4.0 DISCUSSION

4.1 Multi – Tool Approach

In the study of extrusion of aluminum alloys, there are many facets of the process that must be optimized. For example, metal flow, temperature, friction conditions, properties and tolerances must be optimized for a specific alloy and shape. There is no single laboratory test that can simulate all of these different conditions at the same time. Therefore, a multi – tool approach must be taken whereby several conditions of the process can be simulated and compared to others. For example, in this research, the temperature of the material is simulated and undergoes a certain amount of plastic strain. In order to fully characterize the microstructure in terms of crystallographic information, EBSD must be used. When metal flow is characterized for different die designs or friction conditions, physical modeling or even Finite Element Modeling must be used.

4.2 Thermal Cycling and Mechanical Properties

The results for the thermal cycling simulation showed that, in general, for constant time cycles, the higher temperatures of both preheating and extrusion contribute to a more fully solutionized post – extrusion product. Care must be taken so that not too much Mg and Si are in solution by the end of preheating. Long dwell times in the preheat furnace may cause a highly solutionized structure and the flow stress during extrusion may then be too high.

It is apparent that small differences in the thermal history of 6061 produce large differences in the microstructure and mechanical properties. Based on the billet preheat cycles used, it can be seen that not all of the coarse β' Mg_2Si precipitates present in the homogenized structure are solutionized prior to deformation. As a result of higher preheating temperatures, more β' has gone back into solution as can be seen when comparing Figures 20 and 21 for 6061 and 28 and 29 for 6063. These coarse precipitates have been linked with Type II tearing.[24] Type II tearing is initiated at coarse Mg_2Si particles as a result of localized eutectic melting which occurs during deformation. In all thermal cycle scenarios, the AlFeSi precipitates spherodized to a similar degree. When a low preheat temperature is combined with a low deformation temperature, it can be seen that the resultant structure has retained original coarse Mg_2Si precipitates (Figures 22 and 30). The tensile data supports this with a comparatively low yield and ultimate strength value. The fact that the precipitates in the low preheat – low extrusion cycle are coarse and undesirable results in lower tensile values. Bear in mind that these data are based on heat treatment alone and are used for comparison between thermal cycles. Grain size and precipitate shape may be altered during deformation and will produce different mechanical property values. In the low preheat – high extrusion, and high preheat – low extrusion combinations, it can be seen that the microstructure yields a much lower amount of coarse Mg_2Si precipitates (Figures 23, 24, 31, and 32). It can be seen that the higher preheat temperature has had a positive effect on the tensile properties of the material. The high preheat and high extrusion temperature profile yielded the best results, whereby the high extrusion temperature was sufficient in bringing most of the remaining Mg_2Si into solution (Figure 25 and 33). The most solutionized structure yields the highest tensile results. However, higher temperature thermal cycles may be limited by surface tearing or other defects associated with high temperature extrusion. This effect is shown in extrusion limit diagrams. Different areas of the billet undergo different heating rates. Strain gradients, for example, produce temperature gradients, especially in the shear intensive zone. In one billet, different areas may undergo somewhat different thermal cycles. Therefore the resultant microstructure will yield varying distribution of grain size and precipitates. Optical, non - contact pyrometers, or contact probes can serve as indicators of surface temperature. These measurements are made on the extrudate away from the die.[25] However, the center of the extrudate is cooler because of less deformation and no friction between the billet - die and billet – container interfaces.[23] For example, Altan, et. al., performed work on determining the variation in temperature of an Al – Mg alloy in hot extrusion.[26] Figure 46 shows this distribution. Additionally, it is a known fact that heavy sections of extrudate profiles can undergo reverse heating on the run – out table when not quenched properly. This phenomenon is due to the heat transfer from the hotter center of the heavy section to the cooler surface.

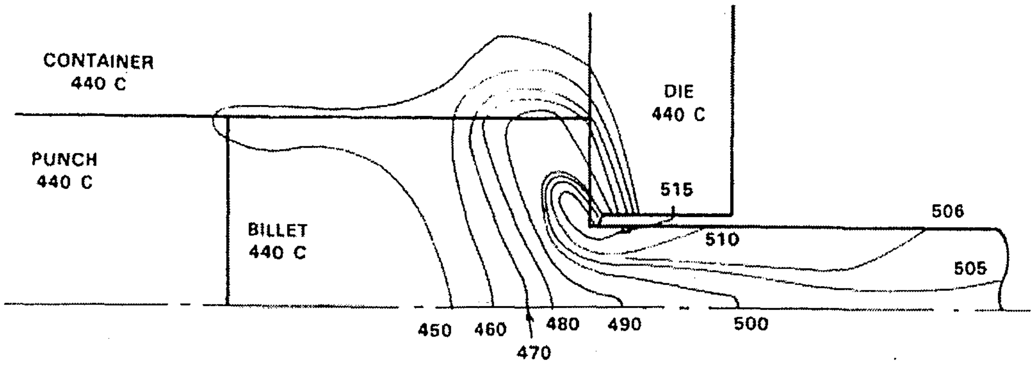

Figure 46: Temperature gradients seen in an Al – Mg alloy in hot extrusion.[26]

Therefore, temperature differences across an extrudate can result in different microstructural characteristics such as varying grain size and precipitate distribution. In large sections, for example, where the local extrusion ratio is low in certain places, the material may not deform significantly. Therefore, the temperature rise due to deformation will be minimal in this case. As a result, the as – extruded properties of the large section of the extrudate will be different than the more deformed areas. Upon ageing, it was seen that the low preheat – low extrusion thermal cycle samples had retained coarse Mg_2Si (Figures 27 and 34). The high preheat – high extrusion thermal cycle had a much more preferable homogeneous distribution of fine Mg_2Si (Figures 26 and 35). This is reflected in the hardness data in Table V.

4.3 Compression Testing and EBSD

An inverse pole figure displays information on the orientation of the grain relative to a reference direction; here, the compression direction. When many results are plotted, the inverse pole figure displays orientation contours, which may show a preferred orientation. The inverse pole figure is much more useful in extrusion because the correlation between the sample axes and extrusion direction can be made much more easily. Previously, pole figures were used to determine orientation in extrusion. However, pole figures are much better suited for forming processes where the deformation is more uniform, such as rolling and drawing. If a strong texture exists in an inverse pole figure, the orientation contours would display a maximum in one of the three principal axes. If a weak or random texture exists, the data would be scattered about the figure. In Figure 43, it can be seen that there is not a significant preferred orientation corresponding to the dead metal zone. This correlates with previous work performed on a partially extruded billet where the dead metal zone showed no preferred orientation.[11] Grains oriented in the <110> crystallographic direction in Zone II (Figure 44) is consistent with previous work on compressed aluminum.[20] The tendency towards the <111> crystallographic direction in Zone III in Figure 45 suggests that the grains are adjusting to the different strain path and increasing strain.

The most dominant slip system in FCC metals is the {111} plane and in the <110> direction. Slip bands form at relatively low strains which is why they appear at the interface between the deformed and undeformed regions of the sample, for example between Zones I and II (Figures 39 and 40).[20]

In an extrudate with a low extrusion ratio, different areas of the deformation zone will be associated with different areas of the extrudate. For example, the surface of the extrudate may incorporate more flow from the intensive shear zone, namely Zone III, while areas closer to the center of the extrudate may see more flow from the area corresponding to Zone II.

4.4 Future Work

The work in this research encompasses an effort to develop methods using a Gleeble thermal – mechanical simulator to accurately predict the microstructure and texture evolution during extrusion of aluminum alloys. However, the thermal cycles in used in this research represent upper and lower bound temperatures for the preheating, extrusion and press quench portions of the process. A more extended database of microstructures and mechanical properties could be developed for a specific alloy while varying the process temperatures and cooling rates.

In addition, compression testing could be used further to predict strain maps of different parts of the billet. Further correlation between actual extrudates, for example surface texture, could then be made using EBSD. In addition, the effect of dynamic recrystallization may be detected using EBSD. However, further work must be performed to improve the pattern quality of the diffraction patterns on deformed aluminum. Possible areas of improvement include the use of electropolishing or chemical polishing to further remove any deformation layer from mechanical grinding.

5.0 CONCLUSIONS

This work has examined methods of simulation for microstructural and textural development during extrusion of 6xxx aluminum alloys. Several conclusions can be drawn from this research:

- The use of the Gleeble thermal – mechanical simulator is ideal for accurate replication of all thermal cycles for hot extrusion of aluminum alloys. Heating and cooling rates can be controlled precisely. Therefore, the prediction of microstructure variations at any step in the process for a particular alloy can be predicted quickly and efficiently. In addition mechanical property information can be gathered at each step in the process.
- It was determined that small changes in the thermal cycles for 6xxx aluminum alloys produce significant changes in the microstructure and mechanical properties. Specifically, a low preheat (545^0C for 6061, 410^0C for 6063) combined with a low extrusion temperature cycle (524^0C for 6061, 496^0C for 6063) resulted in a microstructure that contained coarse Mg_2Si precipitates despite the relatively fast cooling rates. The mechanical properties of samples run through these cycles received the lowest mechanical property values. On the contrary, samples run through the high preheat (510^0C for 6061, 460^0C for 6063) combined with a high extrusion temperature cycle (552^0C for 6061, 560^0C for 6063) resulted in a highly solutionized microstructure ideal for ageing. The mechanical properties of samples run through this thermal cycle were the most desirable. Thermal cycles with a combination of low preheat and high extrusion

temperatures received intermediate values of mechanical properties. Post extrusion ageing showed that samples run through the low preheat – low extrusion thermal cycles had retained coarse precipitates and displayed poor hardness values. The opposite effect was seen for sample run through the high preheat – high extrusion thermal cycles.

- Compression testing on a Gleeble proved to be a good candidate for modeling textural information in extrusion. Strain, strain rate and temperature can be accurately controlled in this case. Crystallographic information from different areas of the sample can be related to the strain associated with different deformation zones in extrusion.
- In compression samples, it was determined that there is no significant texture in the undeformed region associated with the dead metal zone in extrusion. Zone II of the sample exhibited a stronger texture in <110> directions in the direction of compression. Finally, a <111> texture was seen in Zone III associated with the highest strain in the sample.
- Sample preparation proved to be important in samples used for EBSD. A surface that is relatively free from plastic strain and does not receive damage from polishing techniques is required for texture analysis.

6.0 REFERENCES

1. G.E. Dieter, Mechanical Metallurgy, McGraw – Hill, 1986, p. 617.

2. I. J. Polmear, Light Alloys, Halsted Press, 1995, p. 39

3. J. Hatch, Aluminum: Properties and Physical Metallurgy, ASM, Metals Park, OH, 1984.

4. The Aluminum Association, Aluminum Standards and Data, 1993.

5. O. Reiso, "The Effect of Microstructure on the Extrudability of Some Aluminum Alloys", Dr. Tech. Thesis, Norwegian Institute of Technology, Trondheim, 1992.

6. A. J. Bryant, R. Fielding, "Developments in Billet and Extrusion Metallurgy on the Operation of the Extrusion Press", Light Metal Age, April, 1998, pp. 6 – 34.

7. A. N. Anderson, "Physical Metallurgy and Extrusion of 6063 Alloy", Proceedings of the Fifth International Aluminum Extrusion Technology Seminar, ET '92, Vol. 2, p.43 – 56.

8. T.J. King, H.K. McGregor, W.Z. Misiolek, R.N. Wright, "Physical Modeling of Microstructure Response in Aluminum Extrusion", Proceedings of the Fifth International Aluminum Extrusion Technology Seminar, ET '92 Vol. 2, p. 377 – 383.

9. A.K Biswas, B. Regen, A. Steinmetz, "Computer Simulation of Extrusion Press Operation Experience with CADEX, A New Computer Aided Process Optimizing System", Proceedings of the Fifth International Aluminum Extrusion Technology Seminar ET '92, vol.2 p.149 – 155.

10. N.C. Parson, J.D. Hankin, A.J. Bryant, "The Metallurgical Background to the Problems Occurring During the Extrusion of 6xxx Alloys", Proceedings of the Fifth International Aluminum Extrusion Technology Seminar, ET '92, p.14

11. J.A Trogolo, R.M. Kelly, W.Z. Misiolek, "Use of EBSD Technique for Microstructural Characterization of the Deformation Zone in Aluminum Extrusion", Proceedings of the Sixth International Aluminum Extrusion Technology Seminar, ET '96, p.217.

12. W.Z. Misiolek, A. Prats, "Analysis of Metal Flow in Weld Pocket Dies", Proceedings of the Sixth International Aluminum Extrusion Technology Seminar, ET '96, p. 75.

13. W. Durrschnabel, "Der Materialfluss beirn Strangpresses von NE – Metallen," Metall, (22), 1968.

14. H. Valberg, "A Modified Classification System for Metal Flow Adapted to Unlubricated Hot Extrusion of Aluminum and Aluminum Alloys", Proceedings of the Sixth International Aluminum Extrusion Technology Seminar, ET '96 p. 95.

15. K. Laue, H. Stenger, Extrusion, ASM, Metals Park, OH, 1981, p. 9-11.

16. O. Reiso, "The Effect of Composition and Homogenisation Treatment on Extrudability of Al – Mg – Si Alloys" Proceedings of the Third Extrusion Technology Seminar, ET '84, Vol. 1, p.31 – 40.

17. J. Zasadzinski, W. Misiolek, W. Libura, J. Richert, "Modeling of Temperature – Speed Parameters in Aluminum Extrusion", Light Metal Age, 1992, Vol. 7 & 8, p. 60 – 64.

18. Randle V., "Crystallographic Characterization of Planes in the Scanning Electron Microscope", Materials Characterization, vol. 34, 1995, pp. 29-34.

19. TSL OIM Software manual, TexSEM Laboratories, 1998, Draper, UT.

20. M. Hatherly, F. J. Humphreys, Recrystallization and Related Annealing Phenomena, Pergamon, 1995, pp. 43 – 56.

21. L. Poizat, B. Hutchinson, "Simulation of Texture Development During Axisymmetric Compression and Tension," Institutet For Metallforskning, Swedish Institute for Metals Research, reproduced by National Technical Information Service, 1997.

22. Gleeble 1000 HAZ Manual, Dynamic Systems, Inc., Troy, NY.

23. J. Wert, "Modeling of Precipitate Growth and Dissolution in Al-Mg-Si Alloys: Application to Processing of Extrusion Billets", Proceedings of the 5th International Extrusion Technology Seminar, Vol. II, (1992) 393 – 401.

24. H. Gjestland, A.L. Dons, O. Lohne, and O. Reiso, Aluminum Alloys: Their Physical and Mechanical Properties, Engineering Materials Advisory Services, West Midlands, 1986, pp. 359 - 370.

25. Lefstad, M., "Metallurgical Speed Limitations during the Extrusion of Al-Mg-Si Alloys", Dr. Sci. Dissertation, University of Trondheim, 1993.

26. T. Altan, S. Oh, H. Gegel, Metal Forming: Fundamentals and Applications, American Society for Metals, Metals Park, OH, 1983, p. 94.

VITA

William was born to Herman and Annette Van Geertruyden on April 17, 1976 in Pittsburgh, PA. Upon graduating from Berkeley Preparatory School in Tampa, FL in 1994, William began attending Lehigh with interests in engineering. He graduated in 1998 with a Bachelor's degree in Materials Science and Engineering degree. William is presently working on various metal forming projects related to aluminum alloys. William has been a co – author of five conference papers and presented three in the area of aluminum extrusion simulation and characterization. He will be continuing this research as he pursues a Ph.D. in Materials Science and Engineering at Lehigh University.

END OF

TITLE